Exploring Mechanisms of Action in Combinatorial Therapies through Solubility Alterations: Advancing AML Treatment

Elham Gholizadeh[1,ϕ]; Ehsan Zangene[1,ϕ]; Uladzislau Vadadokhau[1]; Danilo Ritz[2]; Juho J. Miettinen[3]; Rabah Soliymani[1]; Marc Baumann[1]; Mathias Wilhelm[4]; Caroline A. Heckman[3]; Amir A. Saei [5,ϱ] and Mohieddin Jafari[1,ϱ,*]

(1) Department of Biochemistry and Developmental Biology, Faculty of Medicine, University of Helsinki, Helsinki, Finland.
(2) Biozentrum, University of Basel, Basel, Switzerland.
(3) Institute for Molecular Medicine Finland (FIMM), Helsinki Institute of Life Science, iCAN Digital Cancer Medicine Flagship, University of Helsinki, Helsinki, Finland.
(4) Technical University of Munich, Munich, Germany..
(5) Center for Translational Microbiome Research, Department of Microbiology, Tumor and Cell Biology, Karolinska Institutet, Stockholm, Sweden.
ϕ These authors contributed as co-first authors.
ϱ These authors contributed as co-last authors.

* Corresponding author:

Mohieddin Jafari,

mohieddin.jafari@helsinki.fi

Abstract

Acute myeloid leukemia (AML) is an aggressive blood cancer with a poor prognosis. Although treatments like allogeneic hematopoietic stem cell transplantation and high-dose chemotherapy can potentially cure younger patients in some cases, challenges such as relapse and treatment-related toxicities remain significant. Combination therapy has been a cornerstone in AML treatment, offering enhanced efficacy by leveraging the synergistic effects of multiple agents. However, high toxicity levels and the genetic heterogeneity of AML complicate the identification of effective and universally applicable drug regimens. To address these challenges, we introduce CoPISA workflow (Proteome Integral Solubility/Stability Alteration Analysis for Combinations), an innovative method designed to study drug-target interactions specifically within combination therapies. CoPISA detects changes in protein solubility/stability that occur only when two drugs are used together, revealing cooperative mechanisms that single-drug treatments cannot achieve. We applied this method to two highly effective and low-toxicity drug combinations in AML, previously introduced by our group: LY3009120-sapanisertib (LS) and ruxolitinib-ulixertinib (RU). CoPISA workflow utilizes advanced proteomic tools to investigate both primary and secondary target effects, providing a deeper understanding of how combination therapies influence multiple signaling pathways to overcome resistance. Furthermore, we propose a novel concept termed “conjunctional inhibition”, where the combined action of drugs induces biological responses that cannot be achieved by individual agents. This approach introduces a transformation in designing combinatorial therapies and offers new directions for more effective treatments in AML and other complex diseases.

Introduction

Acute myeloid leukemia (AML) is an aggressive hematologic malignancy characterized by the clonal expansion of immature myeloid cells in the bone marrow and peripheral blood, resulting in disrupted hematopoiesis. Despite advancements in treatment, the prognosis remains poor, particularly for older adults, with long-term survival rates below 15% for patients over 60 years old[1]. Combinatorial regimens, such as venetoclax with azacitidine (VenAza) or azacitidine with cytarabine (AzaCyt) combinations, have shown promise in improving response rates, particularly for older and less fit patients who may not tolerate high-dose regimens. These combinations leverage synergistic effects to target AML cells more effectively [2,3]. However, challenges such as resistance to these combinatorial therapies emphasize the need for further research to optimize treatment strategies and improve patient outcomes.

Combination therapy has long been a cornerstone of cancer treatment, particularly in hematologic malignancies. This approach often demonstrates superior efficacy compared to monotherapy, leveraging the synergistic or additive effects of different agents to combat complex diseases [4]. On the other hand, recent studies have demonstrated that co-targeting both cancer-specific targets and associated drug-escape mediators can effectively reduce drug resistance in cancers [5]. However, this approach faces several limitations. High toxicity levels often accompany multi-drug regimens, leading to severe side effects that limit therapeutic options [6,7]. Moreover, AML, as a genetically heterogeneous disease, is characterized by each patient's leukemia being driven by distinct mutations and epigenetic alterations. This patient-specific nature of AML makes it challenging to find a "one-size-fits-all" combination therapy [8,9]. The process of identifying optimal drug combinations is further complicated by the vast number of potential therapeutic agents, requiring extensive preclinical and clinical evaluation to assess synergistic effects, dosage optimization, and toxicity management [10]. Additionally, the molecular mechanisms underlying successful combination therapies remain poorly understood, hindering the rational design of new treatment strategies [11].

Recent studies have explored novel methods for elucidating drug-target interactions. One such approach is the study of drug-induced shifts in protein conformational solubility/stability, which can provide insights into the mechanisms of action of therapeutics [12,13]. Thermodynamic-based methods have been developed on this principle and are emerging as promising strategies for drug target identification, particularly because they do not require prior knowledge of the protein targets[14]. The thermal shift assays leverage the principle that drug binding affects a protein's solubility or thermodynamic stability, allowing researchers to identify drug targets across the whole cellular proteome[15]. In this line, PISA assay is a high-throughput technique to monitor drug target engagement and has been employed to decipher the targets of hundreds of drugs recently [15,16,17].

In this work, we explore how drug combinations influence protein solubility/stability, facilitating target deconvolution and enhancing therapeutic outcomes in AML. Central to this study, we introduce CoPISA workflow (Proteome Integral Solubility/Stability Assay for Combinations), an innovative method designed to investigate drug-target interactions specifically within the context of combinatorial therapies. The CoPISA method captures drug interactions by detecting changes in protein solubility/stability that occur specifically when a combination of drugs is used, as compared

to single-drug and control samples. We applied this approach to two recently identified drug combinations with demonstrated high efficacy and low toxicity in AML patients [18]. This technique uses advanced proteomic tools to explore both primary (using lysate sample) and secondary (using living sample) target effects, providing a comprehensive understanding of how combination therapies can modulate multiple signaling pathways to overcome treatment resistance [15,19]. This research extends beyond traditional drug target identification by examining how these interactions impact cellular behavior at a systems level, thereby addressing current limitations in understanding the mechanisms behind successful drug combinations. Moreover, we introduce a novel molecular mechanism termed 'conjunctional inhibition,' where the combined action of drugs produces biological responses that are unattainable by individual compounds (more definition in the Result section). This innovative perspective transforms our understanding of drug interactions and paves the way for more effective therapeutic strategies in AML and other complex diseases.

Results

CoPISA Assay principal and *Ab Initio* Simulaiton

To investigate how combinatorial drug treatments affect protein solubility, we used the CoPISA workflow, an extension of the PISA assay tailored for combination therapies. In the CoPISA assay, we quantify protein solubility/stability by measuring the total amount of each protein, represented as the area under each protein's melting curve (S_m), enabling precise solubility/stability measurements without the need for curve fitting. The CoPISA workflow leverages the high-throughput and high proteome coverage of the PISA protocol and involves treating cells with each drug individually (e.g., A and B), as well as in combination (AB), alongside untreated controls. Lysates or living cells are then subjected to thermal treatment across a temperature gradient to assess shifts in the amount of soluble/stable proteins (S_m) under each condition (**Fig. 1**). Relative changes in S_m compared to the control (ΔS_m) provided quantitative insight into drug-induced effects on protein solubility/stability. These shifts, indicating either stabilization (increased S_m) or destabilization (decreased S_m). Note that in the following, we used "solubility" shift instead of "solubility/stability" to emphasize the change in the amount of soluble protein after altering stability with increasing temperature in the presence and absence of drugs.

The CoPISA workflow enables a detailed analysis of drug-target interactions by classifying proteins into eight classes, revealing distinct impacts on protein solubility. The four trivial classes of proteins according to drug-target interactions can be hypothesized as follows: A (protein targeted by drug A), B (protein targeted by drug B), A∩B (protein targeted by both drug A and drug B), A∪B (protein not targeted by any drug) when using two drugs or compounds for treatment. In one class, some proteins are unaffected by all treatments, showing no changes in solubility compared to control. Two classes involve Independent Inhibition (A or B), where treatment with either drug A or drug B alone leads to specific alterations in solubility profiles, indicating individual effects on protein solubility. These proteins could suggest a synergy mechanism in combinations by targeting two proteins from different or identical biochemical pathways. A∩B represents proteins targeted by both drug A and drug B, where combined treatment results in a distinct solubility shift, potentially indicating cooperative or enhanced binding effects. These proteins could highlight synergistic interactions where the combined action of both drugs leads to a stronger impact than either drug alone.

As a theoretical proof of principle, we conducted a simulation of melting sigmoidal curves for 10,000 hypothetical proteins to explore the possibility of all four classes. This preliminary computational analysis involved randomly selecting melting temperatures T_m in the range from 48 to 56 °C using error (erf) and square root (sqrt) functions. Examples of thus- simulated melting curves are shown in **Fig. 2**. illustrating the variation in thermal stability across the different protein classes. Our analysis suggests that all four expected classes of targeting proteins for this two-drug combination are theoretically possible, based on a normal distribution and hypothetical values for the mean and variance (**Fig. 2A**). This finding supports the idea that different classes of proteins could be differentially affected by the drug combination. In addition, we observed a similar pattern

of these four classes with slightly distinct distribution based on the mean and variance values extracted from a proof of principle TPP published article [20] (**Fig. 2B**), further validating the robustness of our theoretical model and aligning with previously observed experimental data.

However, in the CoPISA workflow, we also consider the treatment of the combination (AB) in addition to the individual drugs. This introduces a unique condition where certain proteins are exclusively targeted by the combination treatment (AB), requiring the simultaneous presence of both drugs to induce significant shifts in solubility. We refer to this as Conjunctional Inhibition. This cooperative effect can be framed within logical gate theory[21], suggesting an AND gate mechanism—both drugs must be present to induce inhibition. This pattern indicates that these proteins may possess multiple binding sites or complex allosteric regulation modulated only by both drugs, providing insights into the underlying mechanisms of this drug combination. Conversely, if a protein is targeted in the presence of A, B, or A∩B, it aligns with an OR gate model, representing an overlap of effects across treatments. This mechanism offers an additional explanation for synergy in drug combinations, where the effects are enhanced when used in tandem compared to monotherapy.

Ultimately, we identified eight classes of proteins. Four of these classes demonstrate shared protein targets across all drug treatments (AB∩A, A∩B, A∩B∩AB, AB∩B), while two classes show individual protein targets specific to drug A or B treatments. One class, termed Conjunctional Inhibition, is uniquely targeted by the combination treatment (AB), and the remaining class consists of proteins that are not targeted by any treatment.

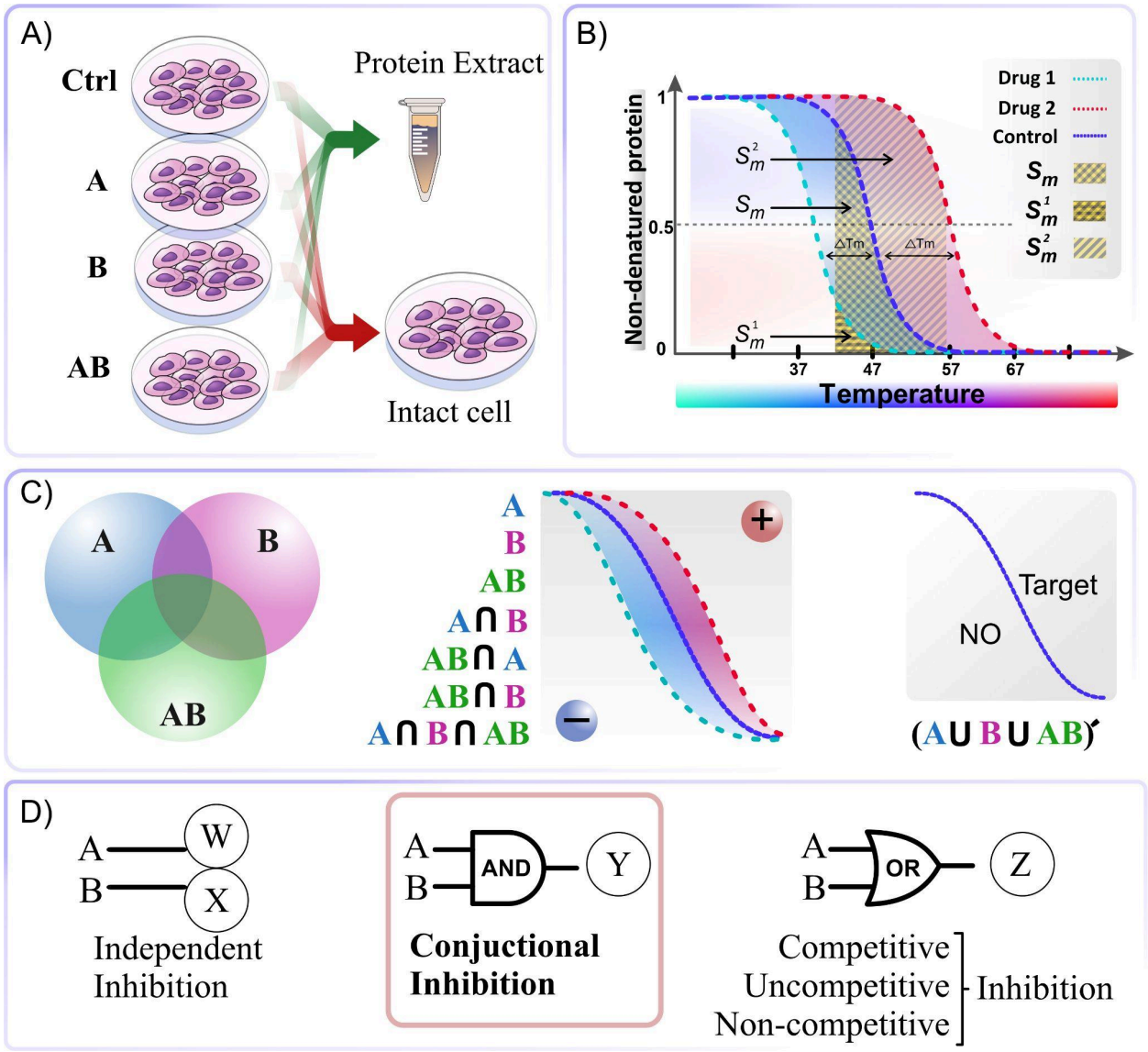

Figure 1: CoPISA workflow and possible states for target discovery in combinatorial therapy. (A) Treatment conditions (Control, Drug A, Drug B, AB combination) are shown, where both living cells and lysate samples are analyzed for temperature-dependent protein solubility shifts. (B) Comparison of PISA concept of integral analysis with the concept of sigmoidal curve fitting when using two drugs. In the PISA workflow, protein solubility shifts are measured based on the area under the curve (ΔS_m) rather than using the median of the fitted sigmoidal curve of denatured protein (ΔT_m) at several temperature points. The area under the curve for the first drug (light blue curve, S_m^1) and the second drug (red curve, S_m^2) is used to calculate ΔS_m within the temperature range of 48–59 °C. The same way is used to measure the area under the curve for the combination treatment. (C) Theoretical illustration of CoPISA concept. This panel illustrates comparisons across multiple single treatments, including drug A, drug B, and combination, and various intersections of these three

treatments (e.g., AB∩A, A∩B, A∩B∩AB, AB∩B). It also highlights cases where no target exists for the union of different treatments. The solubility shifts across these treatment combinations indicate the targeted proteins' interaction. (D) Mapping the three models of drug inhibition to logical gate concepts: Independent Inhibition, where drugs A and B act separately on targets W and X, respectively, corresponds to an independent action; Conjunctional Inhibition, where drugs A and B jointly affect a single target Y, aligns with the AND **logical gate; and Competitive, Uncompetitive, and Non-Competitive Inhibition, representing mechanisms that are either mutually exclusive or involve overlapping inhibition effects, correspond to the** OR **logical gate.**

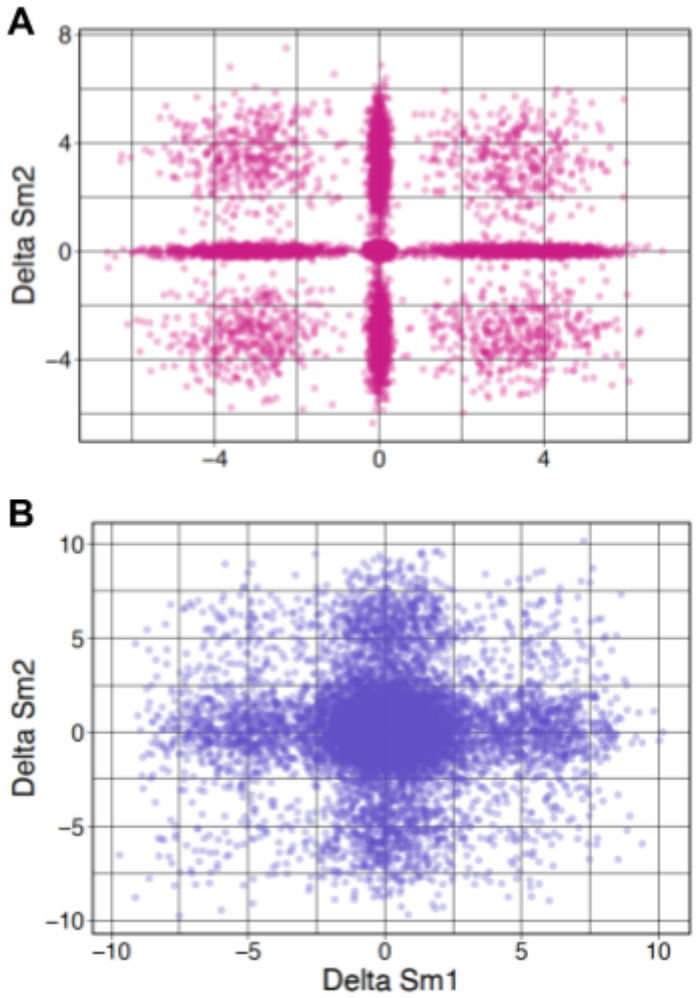

Figure 2: The simulated relationship of protein thermal shift of two hypothetical drugs. (A) ΔS_m^1 **and** ΔS_m^2 **in 10,000 proteins were simulated and depicted using a normal distribution with hypothetical mean and variance and (B) with mean and variance extracted from the proof of principle TPP published article[20].**

CoPISA Analysis of LY3009120-Sapanisertib and Ruxolitinib-Ulixertinib combinations in AML cell lines

Using the CoPISA workflow, we identified protein solubility patterns across single and combination treatments in AML cells treated with LY3009120-sapanisertib (LS) and ruxolitinib-ulixertinib (RU), across both cell lysates and living cell conditions. We identified both potential primary and secondary targets to assess the intracellular effects of these treatments. Across the different experimental conditions, the analysis revealed distinctive patterns of protein targeting, reflecting the cellular responses elicited by each therapeutic approach.

In the LS-treated samples, significant shifts in protein solubility were observed across the single and combination treatments under both living cell and lysate cell extract conditions, as displayed in **Fig. 3A** and **3B**. In the lysate cell extract condition (**Fig. 3A**), treatments with LY3009120, sapanisertib, and the LS combination resulted in 520, 432, and 704 significantly altered proteins, respectively. In contrast, in living cells (**Fig. 3B**), treatments with LY3009120, sapanisertib, and the LS combination yielded 381, 348, and 206 significantly altered proteins, respectively.. These results suggest that, while combination therapy with LS induces a greater number of solubility alterations in the lysates, the living cells condition demonstrates a more restrained, yet still substantial, set of commonly affected proteins, indicative of treatment-specific solubility responses in both cellular states.

Similarly, in the RU-treated samples, a distinct pattern of solubility alterations emerged across treatments with ruxolitinib, ulixertinib, and the RU combination, under both living cell and lysate conditions, as shown in **Fig. 3C** and **3D**. In the living cells condition (**Fig. 3C**), treatment with ruxolitinib, ulixertinib, and the RU combination resulted in 462, 618, and 487 significantly altered proteins, respectively. In the lysate condition (**Fig. 3D**), treatment with ruxolitinib, ulixertinib, and the RU combination yielded 636, 956, and 241 significantly altered proteins, respectively. These findings highlight that, while individual treatments tend to produce extensive alterations in protein solubility, the combination treatment exhibits a more selective pattern of solubility changes, particularly under the lysate condition. Together, these observations underscore the differential impact of single and combined treatments on protein solubility, with notable differences between lysate and living cell conditions that may inform the distinct mechanistic effects of combination therapies on protein dynamics.

Building upon these findings, further analysis of protein solubility shifts in the LS- and RU-treated samples (**Fig. 4**) reveals distinct intracellular effects of each combination therapy. In the samples treated with LS, the solubility of 177 and 107 proteins were significantly shifted in lysates and living cells in the AND gate analysis, suggesting specific intracellular effects of the combination therapy. Also, in the lysate samples treated with RU, 77 proteins with significant solubility shifts were identified as primary targets while 105 were identified in living cell samples as primary and secondary targets. Notably, each treatment condition included some overlapping proteins identified in both living cell and lysate samples, suggesting shared mechanisms that may consistently affect cellular pathways across different cellular states.

To ensure the robustness of the significance cutoff and to effectively control the false discovery rate (FDR) for solubility shifts, a comprehensive permutation analysis of protein S_m values was conducted. The analysis demonstrated that, on average, the FDR across all analyses was maintained at 2%, ensuring the reliability of the identified significant solubility shifts.

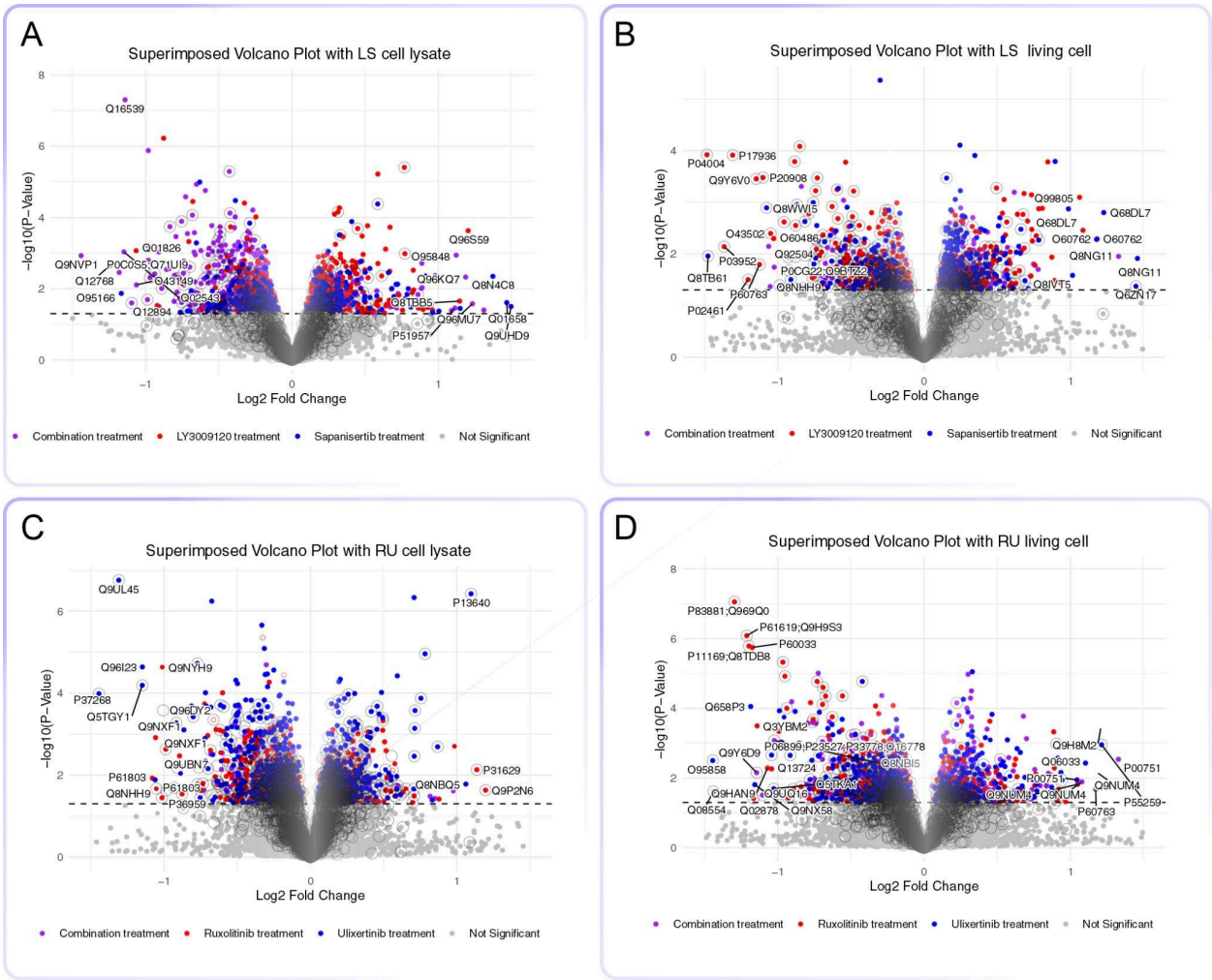

Figure 3. Volcano plots illustrate identified targets in the CoPISA method for lysate cell and living cell treatments with both drug combinations. Each plot is a superimposition of three comparisons between control and treatment groups, with solubility shifts indicated by different colors: lysate cell samples (A) and living cells (B) treated with LY3009120 (500nM) (red), sapanisertib (500nM)(blue), and their combination, LS (purple); and lysate cell samples (C) and living cells (D) treated with ruxolitinib (3uM)(red), ulixertinib (3uM)(blue), and their combination, RU (purple). Dots with black outlines represent proteins uniquely identified in the corresponding treatment.

Intersectional Target Analysis of Protein Solubility Shifts in Lysate and Living Cell Samples

The intersection analysis revealed proteins consistently targeted across both living cells and cell lysate samples indicating a comprehensive coverage of the drug's actions on cellular pathways, potentially impacting multiple cellular processes. In samples treated with LY3009120, 11 proteins with significant solubility shifts were consistently detected in both living cells and cell lysate samples (**Fig. 4**). Among these, the presence of mitogen-activated protein kinase (MAP3K20)

suggests the involvement of MAPK signaling pathways in the therapeutic response. This indicates that LY3009120 may inhibit key signaling processes, thereby limiting the proliferation and survival of AML cells [22]. The presence of procollagen-lysine dioxygenase (PLOD1) points to potential effects on the tumor microenvironment, possibly altering leukemia cell interactions with surrounding tissues [23]. Additionally, the neutral amino acid transporter (SLC1A5) indicates that the drug may influence amino acid metabolism, which is critical for cellular growth [24]. Derlin-1 highlights a mechanism related to protein quality control disruption, which could increase endoplasmic reticulum stress in leukemia cells, contributing to cell death [25].

In samples treated with sapanisertib, two proteins show significant solubility change in both the living cell and lysate cells that are linked to ribosomal function and protein synthesis. Targeting these processes could restrict AML cell proliferation by disrupting their ability to synthesize proteins essential for survival [26]. The detection of histidine decarboxylase (HDC) as a target could suggest an impact on histamine signaling pathways, potentially modulating immune responses, and influencing the tumor microenvironment to enhance treatment efficacy [27].

Three proteins were targeted in the "OR" gate condition, common to both living cells and cell lysate forms. The presence of plexin-C1 as a target indicates that the treatment with any of LY3009120 or sapanisertib may affect cell signaling related to cell motility and adhesion, potentially influencing how AML cells migrate and interact with the bone marrow microenvironment [28]. Protein disulfide-isomerase TMX3 highlights a potential mechanism of endoplasmic reticulum stress induction, suggesting that the treatment may exploit this pathway to induce cell death in leukemia cells [29]. The detection of dolichyl-diphosphooligosaccharide-protein glycosyltransferase (DDOST) as a target for LS treated samples in "OR" gate suggests that glycosylation processes may be altered, impacting protein solubility and function, which could further contribute to the therapeutic effects of the treatment [29].

Under the AND gate, four proteins are targeted in samples treated with the combination of LS, in both living cell and lysate samples. The mitochondrial proton/calcium exchanger protein (LETM1) indicates that the combination therapy may modulate mitochondrial function and calcium homeostasis, which are crucial for maintaining apoptotic pathways in AML cells [30]. This modulation could potentially enhance the sensitivity of cancer cells to apoptosis. Additionally, the small integral membrane protein (SMIM24) suggests that drug-induced changes in membrane dynamics could influence drug uptake and intracellular transport, enhancing therapeutic efficacy [31]. The presence of the ribosomal subunit protein uS2m as a target implies that the combination may affect protein synthesis, disrupting AML cell proliferation. Lastly, the combination treatment with LS led to solubilization of 8-oxo-dGDP phosphatase (NUDT18) suggesting an increased targeting of oxidative stress and DNA repair pathways, enhancing the therapeutic effects of the combination therapy by increasing the susceptibility of leukemic cells to DNA damage [32]. This integrated approach highlights the potential of LY3009120 and sapanisertib combination treatment to disrupt multiple cellular processes essential for AML cell survival.

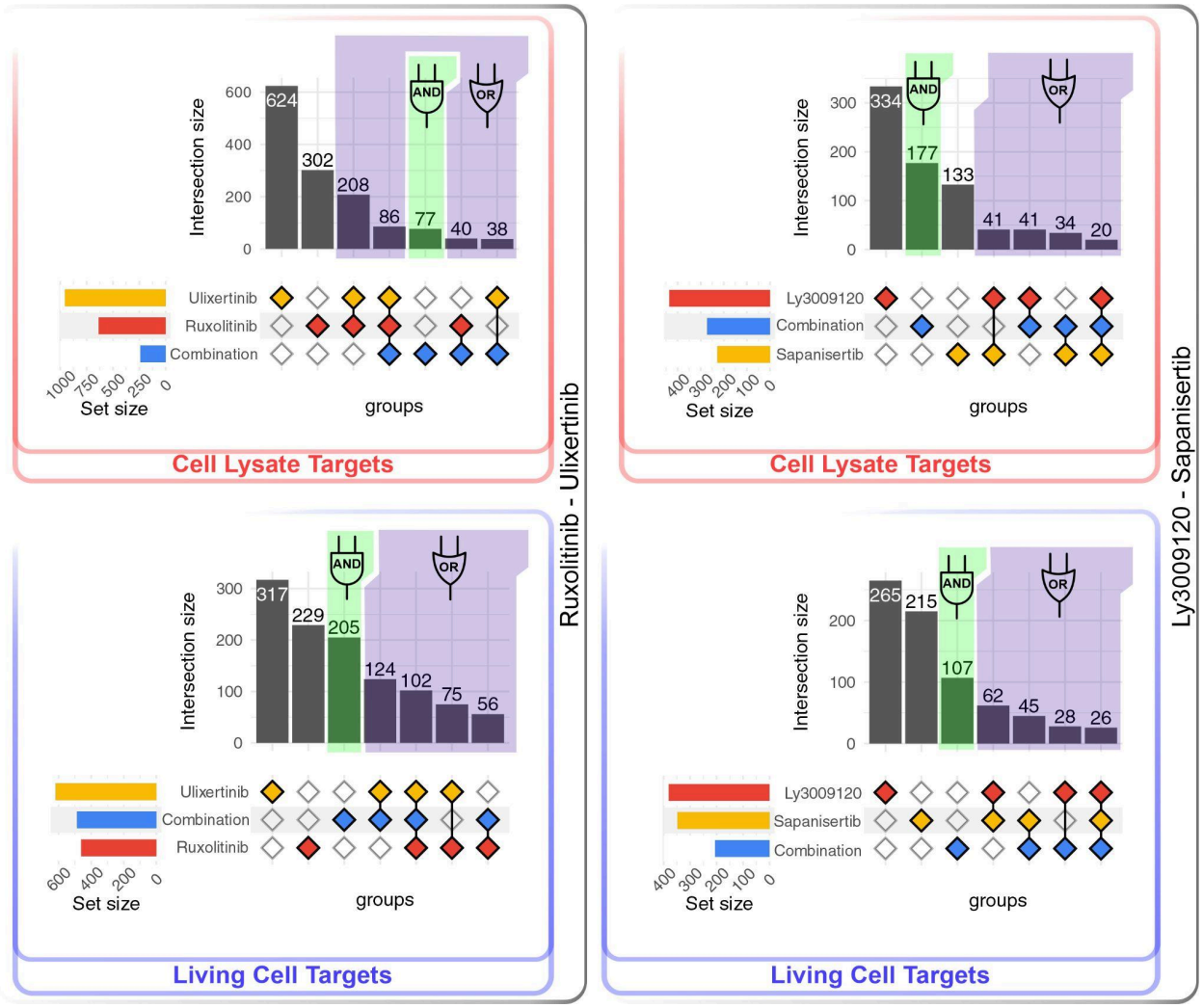

Figure 4: Upset plots display the number of identified target IDs in the lysate (representing primary targets) and living cell samples (encompassing both primary and secondary targets) for LY3009120-sapanisertib and ruxolitinib-ulixertinib treatments.

In the ruxolitinib-treated samples, seven proteins were targeted in both living cell and lysate samples (**Fig. 4**). Notable proteins such as RNA-binding protein and Dysferlin play significant roles in modulating cellular responses. RNA-binding proteins are essential for alternative splicing and regulation of gene expression, suggesting that ruxolitinib may impact splicing mechanisms critical for AML cell proliferation [33]. Dysferlin, on the other hand, is implicated in membrane repair and muscle cell integrity, indicating a possible role in maintaining cellular homeostasis during therapeutic stress [34]. The identification of these proteins emphasizes how ruxolitinib may alter gene expression and cellular responses, potentially enhancing its therapeutic effects in AML.

In ulixertinib-treated samples, two known targets from the DrugBank database were identified in the lysate samples: mitogen-activated protein kinases 3 and 1 (MAPK3, MAPK1), which are essential components of the MAP kinase signal transduction pathway [35]. Across both Lysate and living cells, ulixertinib commonly affected 22 proteins. Key proteins such as RNA polymerase II and mitogen-activated protein kinase (MAPK9) are included in this group. RNA polymerase II is crucial for transcribing mRNA, which might highlight ulixertinib's role in regulating gene expression

necessary for AML cell survival [36]. Furthermore, MAPK9 is involved in signaling pathways that control cellular growth and differentiation, indicating that ulixertinib may disrupt critical signaling pathways in AML [35]. The presence of these proteins suggests that ulixertinib targets transcriptional and signaling mechanisms, potentially enhancing the overall anti-leukemic activity of the combination therapies.

The "OR" gate, 21 protein targets are shared among various conditions in lysate and living cells. Proteins such as C4b-binding protein and proto-oncogene tyrosine-protein kinase Src are significant members of this group. C4b-binding protein is involved in the regulation of the immune response, indicating that these therapies might modulate immune pathways to enhance anti-leukemic effects [37]. Additionally, Src kinase plays a role in signaling pathways that regulate cell growth and survival, suggesting that targeting this protein may help in overcoming resistance mechanisms in AML [38]. The presence of these proteins illustrates how treatment of ruxolitinib and ulixertinib can simultaneously affect immune and growth signaling pathways, potentially leading to improved treatment outcomes in AML.

Finally, the protein targeted in the lysate and living cell treated with the combination of RU is NADH dehydrogenase (NDUFA8). This protein is essential for mitochondrial function and energy production. This observation potentially indicates that combination therapy enhances mitochondrial bioenergetics, potentially leading to increased apoptosis in AML cells. The involvement of NADH dehydrogenase in cellular respiration underscores its potential as a potential therapeutic target to improve treatment efficacy [39]. Moreover, the shared presence of this protein across conditions indicates that maintaining mitochondrial function could be crucial for the conjunctional effects observed in combination therapies.

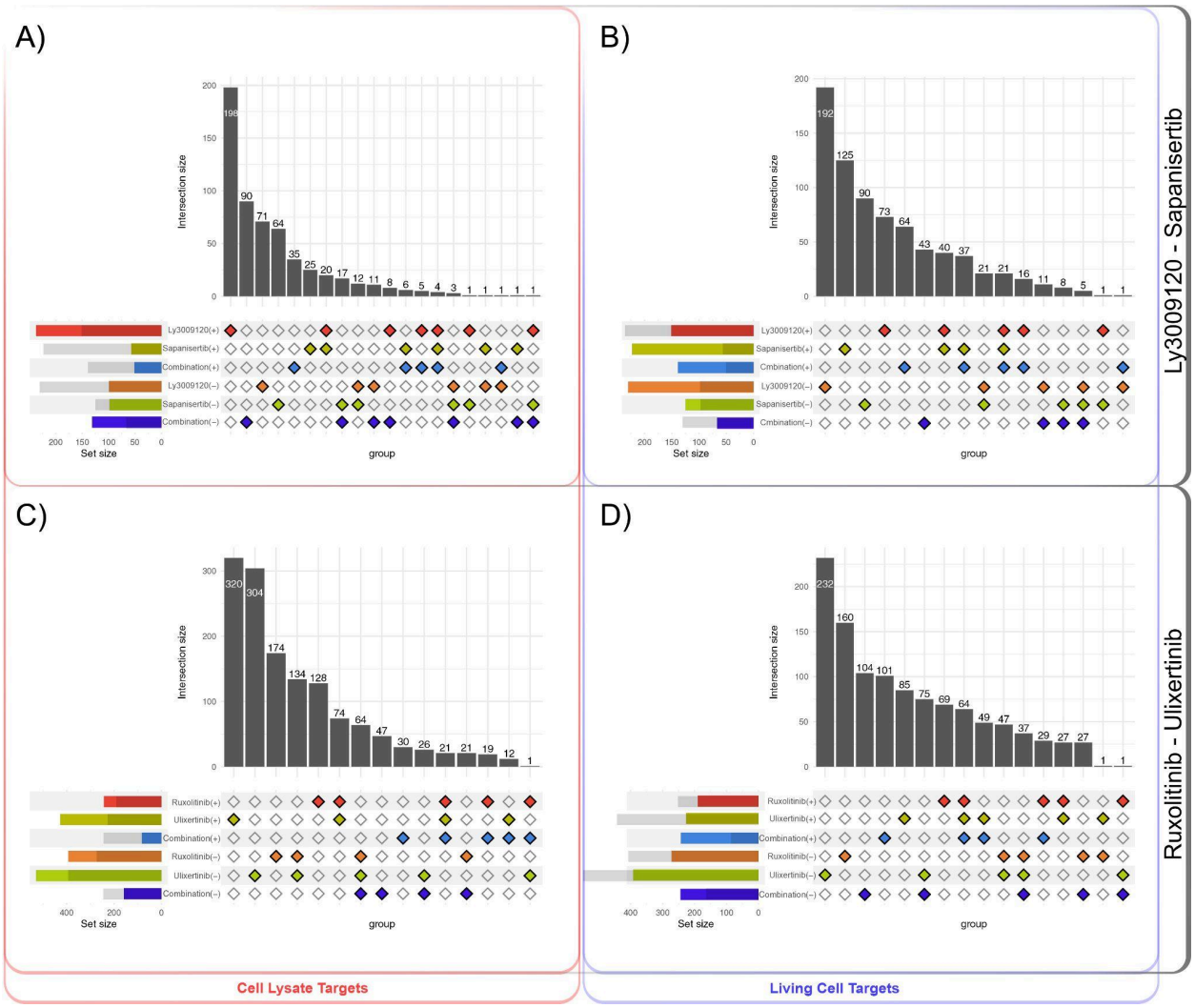

Figure 5: Upset plots showing the number of protein target IDs with altered solubility. The Upset plots illustrate the number of significantly stabilized and destabilized protein target IDs for the combinations LY3009120-sapanisertib (A and B) and ruxolitinib-ulixertinib (C and D) with both living cell (primary + secondary targets) and lysed cell (primary targets) conditions. Stabilized and destabilized proteins are indicated with '+' and '-' symbols, respectively, showing the direction of ΔSm relative to the control groups. For example, "combination(-)" refers to proteins that were destabilized after interaction with the drug combination, while "combination(+)" refers to proteins that were stabilized following interaction with the drug combination. The plots also reveal proteins unique to each treatment and type of alteration, with color-coded bars representing the set sizes and labeled intersections indicating unique and overlapping protein changes among treatment groups. The horizontal bar plots are sorted in semantic order, presenting destabilized and stabilized proteins for single drugs and combinations. To facilitate comparison between living cells and cell lysates, gray bars are used to highlight the respective categories in the bar plots.

The upset plots in **Fig. 5** serves as a verification tool, identifying protein targets with solubility shifts specifically in response to combination therapy, providing finer resolution on the directionality of these shifts. Proteins with enhanced ("+") and reduced("-") solubility are marked relative to control groups, helping to discern how combination treatments influence protein solubility compared to single-drug treatments. For instance, in the RU lysate condition, the combination of RU reveals a coherent stabilizing effect on 21 proteins, where solubility shifts are consistent across both the combination and individual therapies. This detailed visualization allows for a clearer understanding of unique and overlapping protein solubility changes across treatments.

To further investigate the association patterns in protein solubility alterations induced by combination treatments, we generated Fold Change-Fold Change (FCFC) plots (**Fig. 6**). These plots compare the solubility alterations in proteins for each combination treatment relative to the effects observed with the individual drugs alone. Specifically, the FC-FC analysis examines: (1) combination vs. drug1 (e.g., LS combination vs. LY3009120 alone), (2) combination vs. drug2 (e.g., LS combination vs. sapanisertib alone), and (3) drug1 vs. drug2 (comparison between the individual drugs themselves, e.g., LY3009120 vs. sapanisertib). Interestingly, only 0.84% of protein alterations exhibit inconsistent directional changes, where stabilization or destabilization patterns differ between combination and single-drug treatments. This finding highlights a strong alignment between the solubility alteration patterns induced by the combination treatments and those observed for individual drugs, particularly from a stabilization perspective. These results reinforce the idea that combination treatments largely maintain the stabilization directionality of the single drugs, providing further evidence of their targeted and coordinated action on protein solubility.

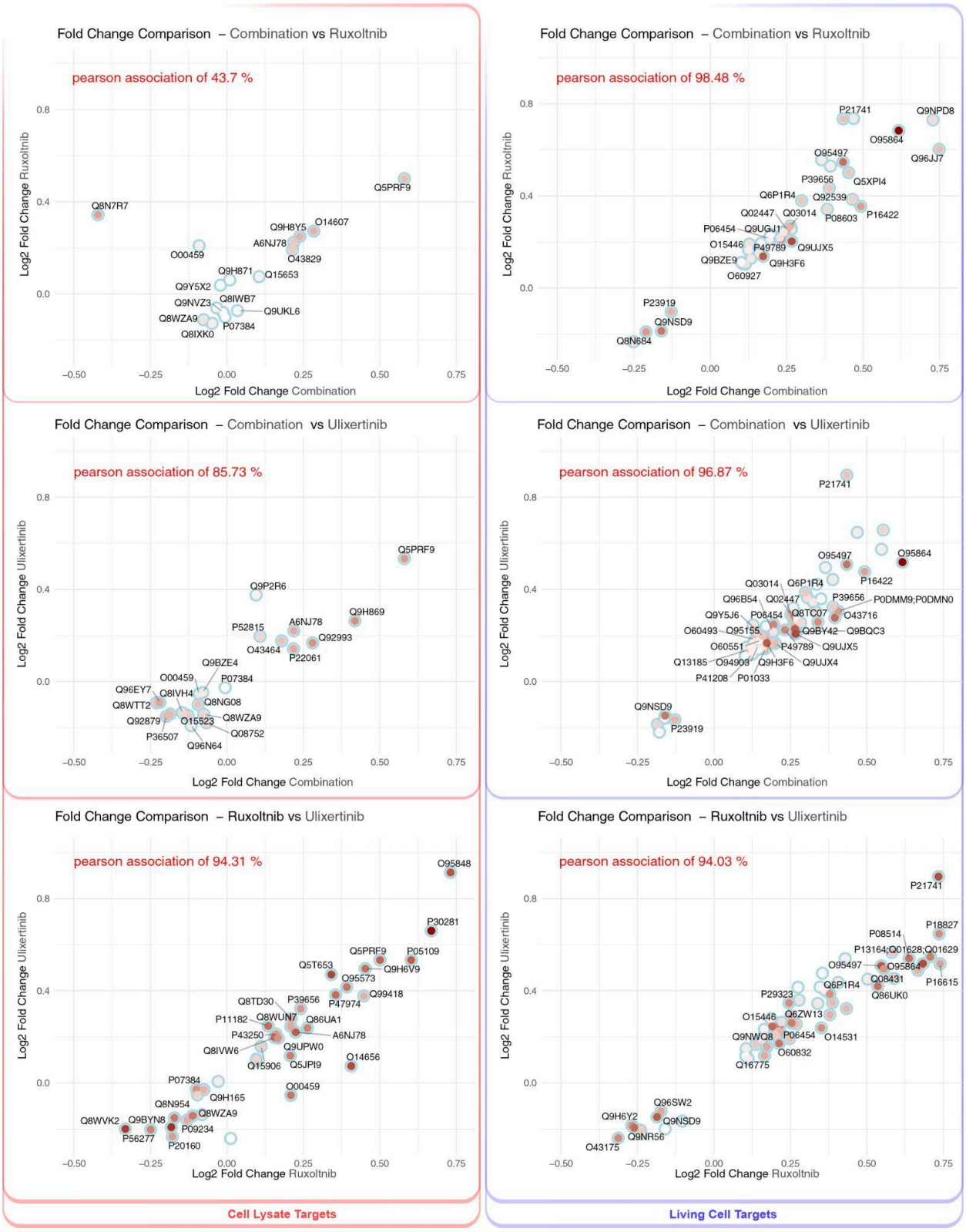
Fold Change Comparison – Combination vs Ruxoltnib
pearson association of 43.7 %
Log2 Fold Change Ruxoltnib
Log2 Fold Change Combination
Fold Change Comparison – Combination vs Ruxoltnib
pearson association of 98.48 %
Log2 Fold Change Ruxoltnib
Log2 Fold Change Combination
Fold Change Comparison – Combination vs Ulixertinib
pearson association of 85.73 %
Log2 Fold Change Ulixertinib
Log2 Fold Change Combination
Fold Change Comparison – Combination vs Ulixertinib
pearson association of 96.87 %
Log2 Fold Change Ulixertinib
Log2 Fold Change Combination
Fold Change Comparison – Ruxoltnib vs Ulixertinib
pearson association of 94.31 %
Log2 Fold Change Ulixertinib
Log2 Fold Change Ruxoltnib
Fold Change Comparison – Ruxoltnib vs Ulixertinib
pearson association of 94.03 %
Log2 Fold Change Ulixertinib
Log2 Fold Change Ruxoltnib
Cell Lysate Targets
Living Cell Targets

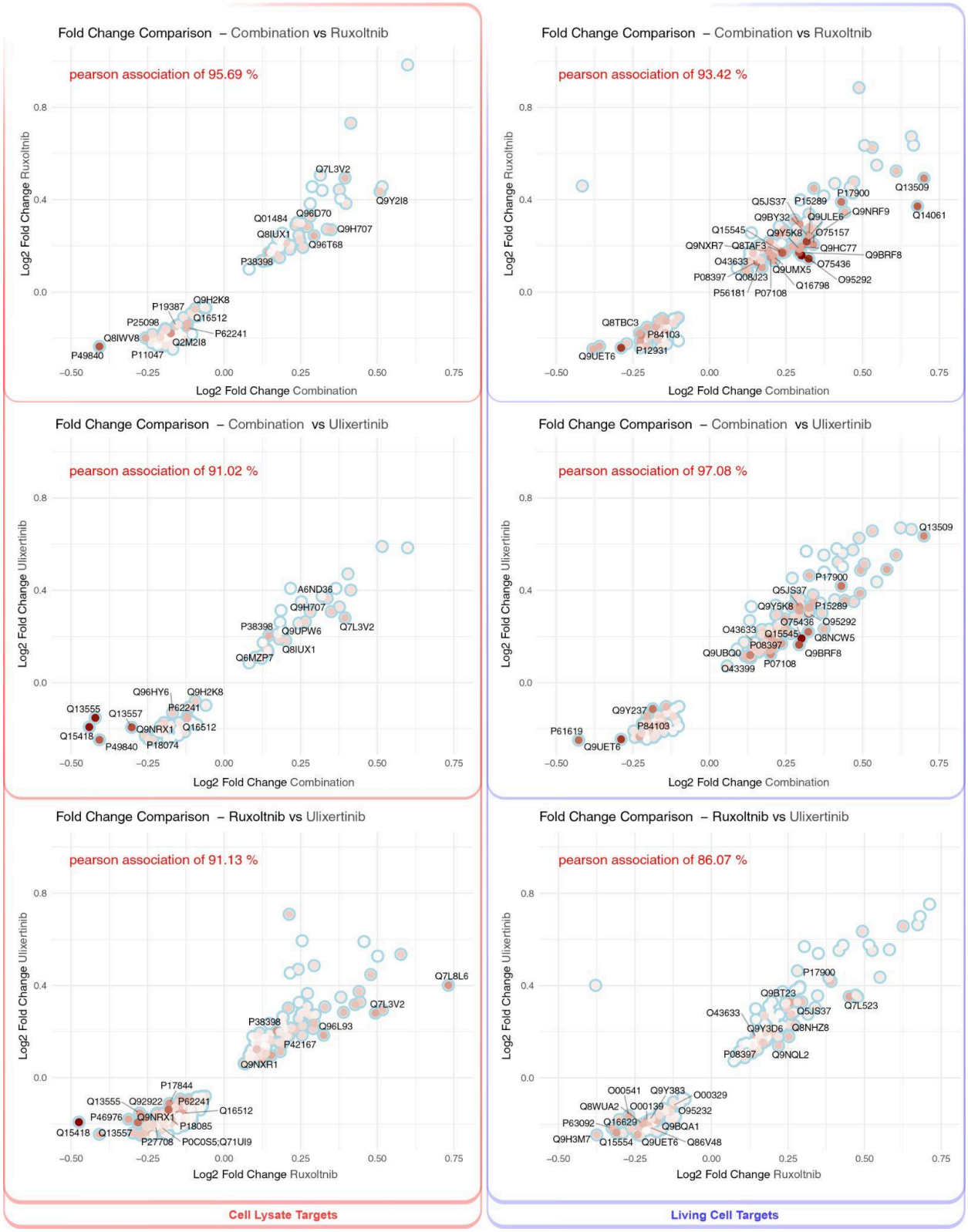

Figure 6: Pairwise fold change comparisons of treatment conditions based on significant proteins. The FC-FC plots display common protein target IDs with fold change values for each

treatment relative to control samples. These plots are presented separately for cell lysate and living cells, with distinct panels for each combination.

Exploring Drug-Drug Interactions Through Mass Spectrometry Analysis

In the next phase, we investigated noncovalent potential interactions or unexpected reactions within the selected drug combinations to confirm that each compound's effects on protein solubility were independent and specific. Using LC-MS/MS analysis[40], we compared the spectral profiles of each drug alone with those of the combined treatments (**Fig. 7**). By analyzing the MS1 spectra and extracted ion chromatograms (XICs) of each compound separately and in combination, we assessed whether a new profile emerges from reacting or interacting drug molecules.

The XICs and MS1 spectra of the combined drugs showed no other peaks or mass shifts other than initial single drug ion peaks, indicating absence of detectable interactions or reactions between the compounds or their modification. Additionally, principal component analysis (PCA) analysis of the whole MS1 spectra provided a comparative view of each drug combination. This analysis confirmed that the effects observed on protein targets were attributable to each drug's specific mechanisms, rather than nonspecific interactions within the combinations. Each compound displayed stable peak intensities and retention times across conditions.

These findings substantiate that the hypothesis the identified protein targets for the LS and RU combinations result from the targeted, independent actions of each drug acting simultaneously, rather than from non-specific interactions between the two drugs. This supports the proposed "AND gate" inhibition mechanism in combinatorial therapy, suggesting these combinations achieve synergistic effects through coordinated drug action and engagement of new signaling pathways.

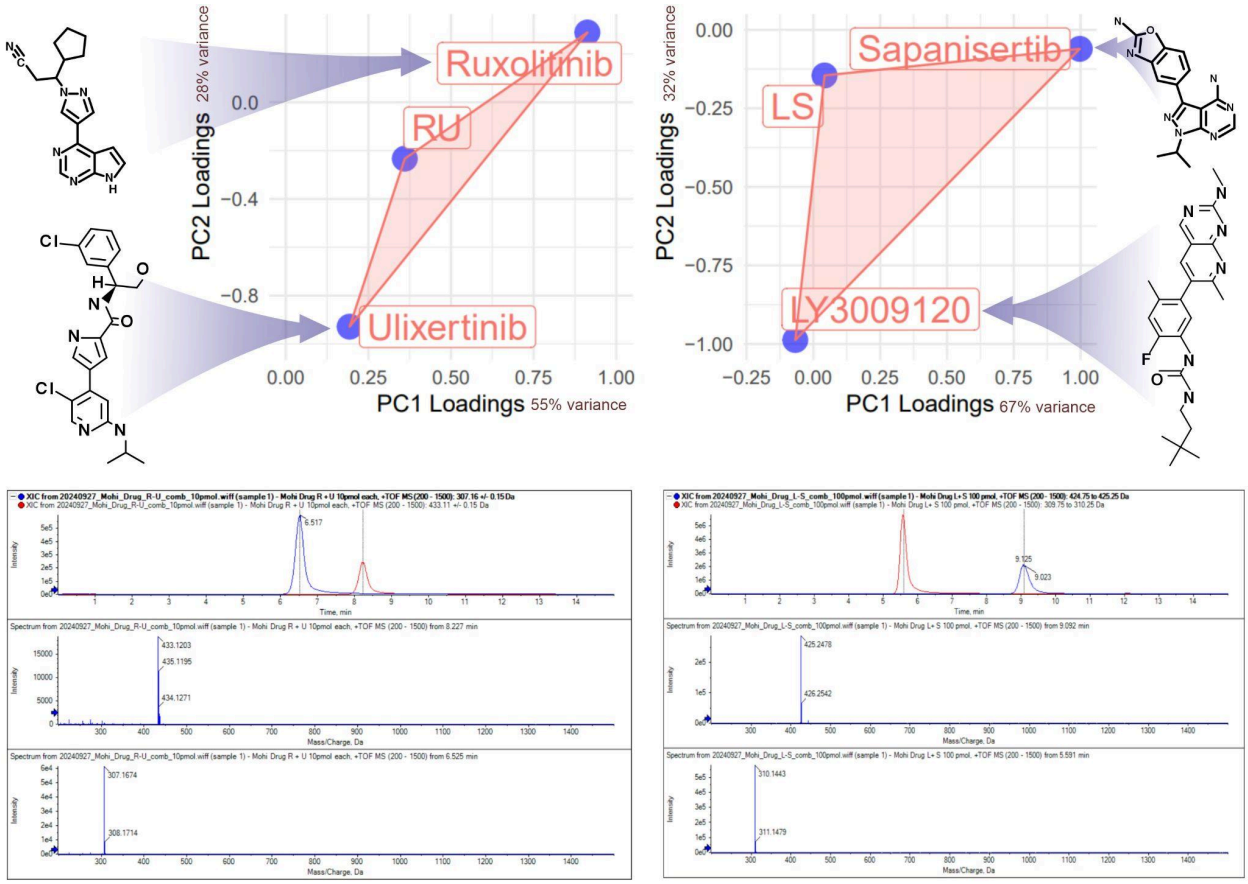

Figure 7: Mass spectrometry analysis of four individual compounds and their combinations. Molecular structures of each compound are shown alongside their MS1 spectra and TICs for the combined samples. PCA loading plots illustrate the distribution of individual compounds and their combinations on PC1 and PC2, based on quantified MS peak intensities.

Pathway Enrichment Analysis in Single Treatments and Intersectional Targets in lysate and living cell Samples

In our study, we perform a comprehensive analysis of the primary, secondary, and overlapping targets of LY3009120 in the AML cell lines, distinguishing the pathways affected in living cells versus lysate samples. In lysate samples alone, 323 proteins were targeted, and 254 specifically targeted upon living cells treatment with LY3009120, with 11 common proteins between living cell and lysate samples (**Fig. 4, Supplementary File 1**). Identified primary targets of LY3009120, significantly impacts pathways involved in protein synthesis and degradation**,** as previously indicated in the literature [41]. Pathways such as Translation and tRNA Aminoacylation are significantly enriched, suggesting a potential disruption of protein synthesis and folding. Furthermore, pathways associated with cellular stress responses, such as hypoxia, are notably affected, highlighting LY3009120's ability to disrupt protein homeostasis and induce cellular stress, leading to cell death [42]. In living cell samples, LY3009120 targets key proteins linked to chromatin modification and epigenetic regulation, processes central to AML pathogenesis (**Fig. 8A**). Enriched pathways including RMTs methylating histone arginines, HDACs deacetylating histones, and chromatin organization, suggesting LY3009120's role in regulating gene expression and chromatin structure in AML [43]. Additionally, pathways related to DNA damage response, cell cycle regulation, and RNA processing are also impacted. The 11 intersecting proteins across living cells and lysate samples provide insight into pathways that LY3009120 may affect consistently, regardless of sample preparation, revealing mechanisms of action that may be central to its anti-cancer effects (**Fig. 8B**). These targets reveales several key pathways, including glycogen metabolism, extracellular matrix organization, and RET signaling [44].

In summary, while lysate-only pathways emphasize protein synthesis disruption and living cell-only pathways highlight chromatin regulation, the intersecting pathways underscore LY3009120's miscellaneous impact on AML cells by consistently modulating energy metabolism, cellular environment, and signaling. These intersecting pathways suggest additional layers of therapeutic impact, positioning LY3009120 as a promising agent targeting both epigenetic regulation and fundamental metabolic processes in AML.

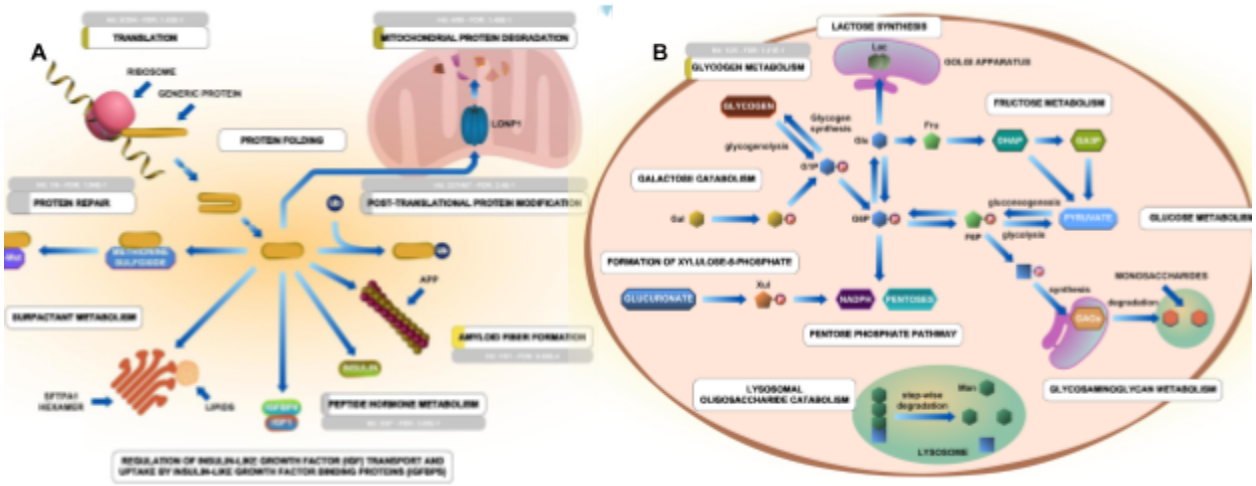

Figure 8. Pathways Enriched in Protein Targets of LY3009120 in AML Cells. A: Pathways related to protein metabolism enriched in living cell samples treated with LY3009120. B: Carbohydrate metabolism pathways enriched in both living cells and lysate samples, including glycolysis, glycogen metabolism, and the pentose phosphate pathway. Data sourced from the Reactome database.

When analyzing the effects of sapanisertib, 213 proteins are targeted in lysate and 131 are targeted in living cells, with only two proteins overlapping between the two sample types (**Fig. 3, Supplementary File 1**). The lysate-specific targets, which represent primary targets of sapanisertib, show significant enrichment in pathways associated with immune cell signaling (**Fig. 8A**). Significantly enriched pathways including KIT signaling, CD28 co-stimulation, and CTLA4 inhibitory signaling, suggesting a potential modulation of immune cell activation and inhibition [45]. This profile points to a possible enhancement of anti-tumor immune responses, particularly through the modulation of cytokine signaling pathways such as interleukin-2 signaling, which could support immune cell function within the tumor microenvironment [46]. Proteins targeted by sapanisertib in living cells are involved in various cellular processes, including protein folding, RNA processing, and apoptosis. Notably, the regulation of MITF-M-dependent genes involved in apoptosis underscores its potential role in mediating apoptotic processes relevant to AML therapy [47]. Pathways such as Translation and Chaperonin-mediated protein folding are significantly enriched, suggesting a potential impact on protein synthesis and quality control. Additionally, pathways related to DNA repair and cell cycle regulation, such as TP53-regulated transcription of DNA repair genes, arealso impacted. These findings suggest that sapanisertib might exert its therapeutic effects by modulating protein synthesis, DNA repair, and cell cycle progression, ultimately promoting apoptosis.

The intersection of targets in both living cell and lysate samples reveals pathways linked to fundamental cellular processes such as histidine catabolism and rRNA processing (**Fig. 9B**) [48]. These overlapping pathways indicate that sapanisertib may exert consistent effects on amino acid metabolism and protein synthesis across different cellular contexts. The enrichment of histidine catabolism suggests alterations in amino acid metabolism, a pathway often co-opted by cancer cells to fuel rapid growth and proliferation [49]. The impact on rRNA processing suggests that sapanisertib could impair ribosomal function, hindering protein synthesis essential for cell survival and proliferation. Comparing the unique and intersecting pathways, lysate-only targets indicate a prominent role for immune modulation, aligning with pathways that may enhance anti-tumor immunity. Living cells-only targets emphasize pathways linked to protein quality control and apoptosis, suggesting that sapanisertib's effects in these samples are more directly tied to inducing cellular stress and programmed cell death. The intersecting pathways, however, suggest a consistent influence of sapanisertib on metabolism and protein synthesis across both sample types, highlighting its broad impact on essential cancer cell functions that support survival and growth. This comparison underscores sapanisertib's multifaceted approach in AML therapy, balancing immune modulation with the direct disruption of cancer cell metabolism and protein synthesis.

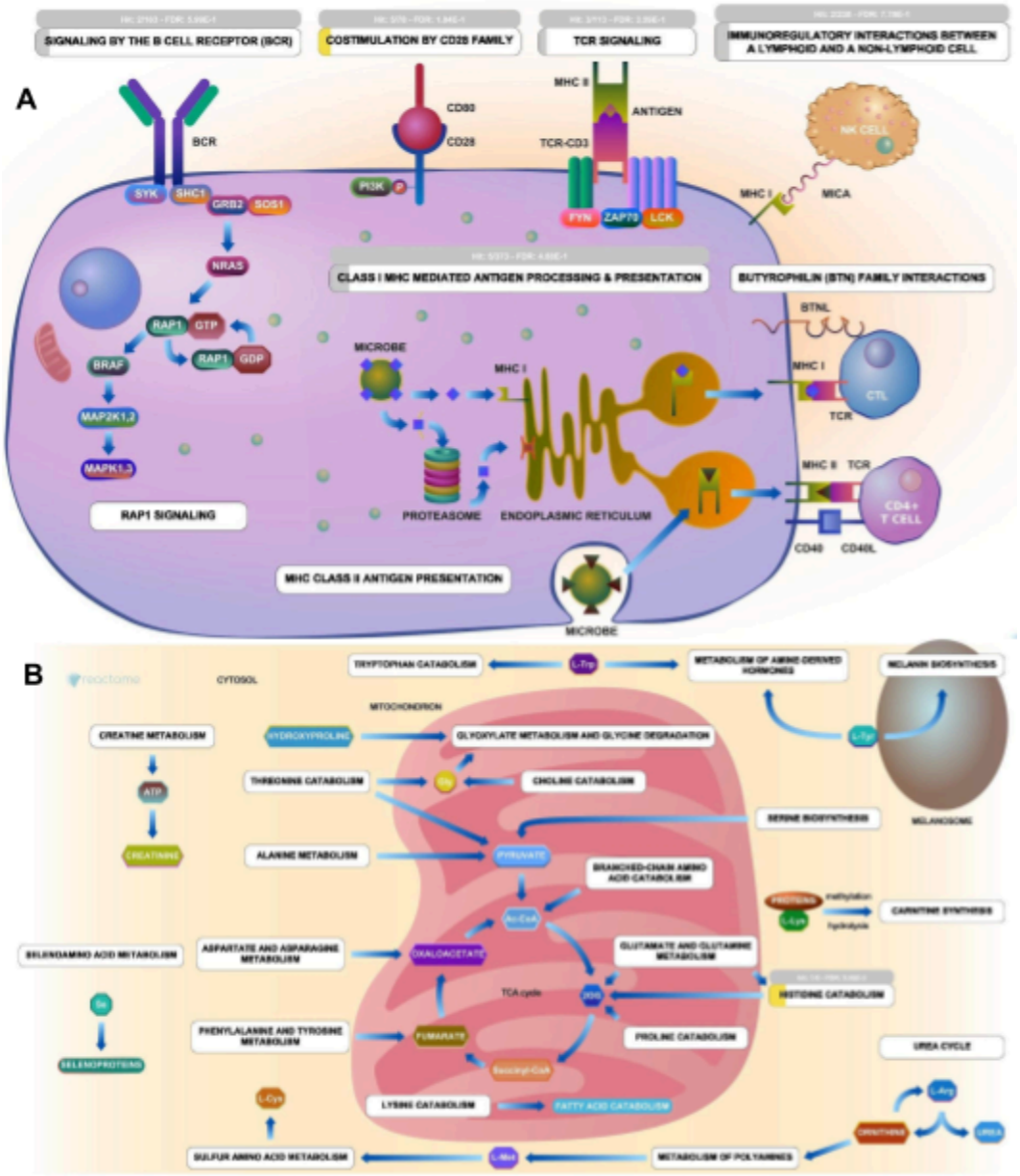

Figure 9. Pathways Targeted by sapanisertib in AML Cells. (A) Adaptive Immune System pathways enriched in lysate samples treated with sapanisertib. (B) Amino Acid Metabolism pathways enriched in the intersection of both living cells and lysate samples. The figure is sourced from the Reactome database

In cells treated with ruxolitinib 295 proteins are targeted in lysate samples and 222 were targeted in living cell samples, with 7 proteins common to both. Ruxolitinib primarily targeted proteins involved in rRNA processing in lysate samples. Significantly enriched pathways included rRNA processing in the nucleus and cytosol, and rRNA modification in the nucleus and cytosol (**Fig. 9**). These findings suggest that ruxolitinib could disrupt protein synthesis by targeting the machinery responsible for ribosome biogenesis [50]. This could lead to impaired cell growth and proliferation, ultimately contributing to the therapeutic effects of ruxolitinib in AML.

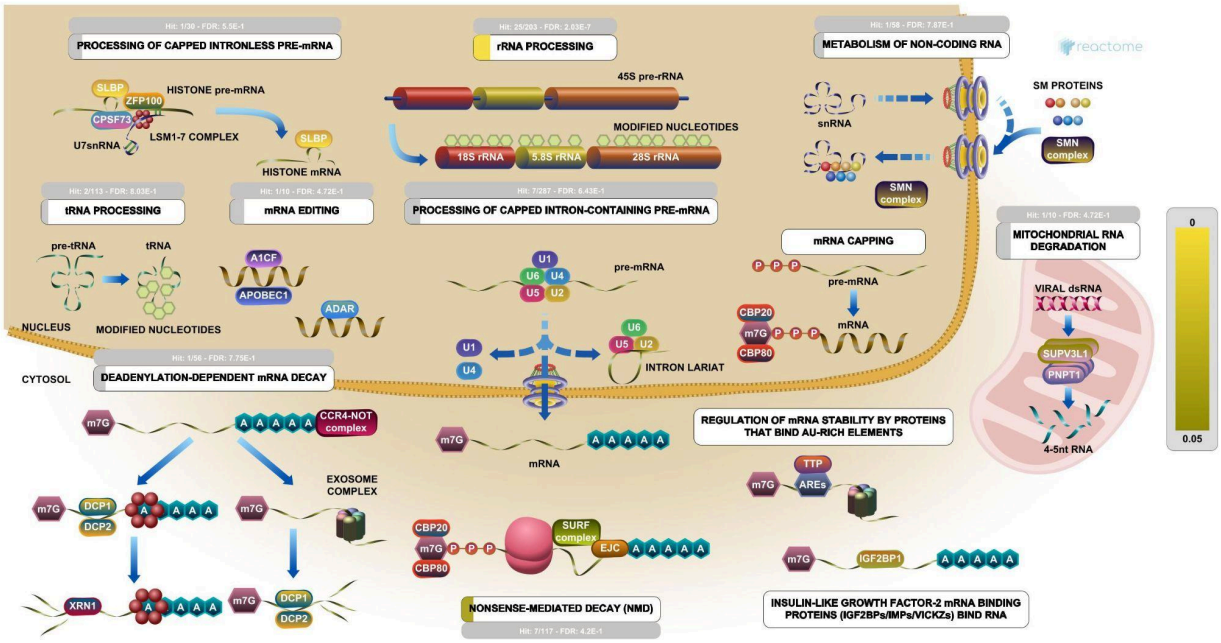

Figure 10. Pathways Targeted by ruxolitinib in AML Cells. This figure is exported directly from the Reactome database.

In the living cell samples, ruxolitinib targets a broader array of pathways, impacting processes such as protein synthesis, cell cycle regulation, DNA repair, and epigenetic regulation. Key enriched pathways including SRP-dependent cotranslational protein targeting to membrane and peptide chain elongation, are identified, suggesting a potential impact on protein synthesis, which is crucial in cancer cell survival and proliferation. Additionally, pathways such as Eukaryotic Translation Termination and Nonsense Mediated Decay highlight the dysregulation of mRNA processing in cancer. Additionally, pathways related to epigenetic regulation, such as histone modifications and chromatin organization, are also impacted [51]. These findings imply that ruxolitinib might exert its therapeutic effects by modulating multiple cellular processes, including protein synthesis, cell cycle regulation, DNA repair, and epigenetic regulation, ultimately leading to cell death and tumor growth inhibition.

When examining proteins targeted in both living cells and lysate samples, ruxolitinib revealed significant enrichment in RNA processing and editing pathways, essential for AML cell survival and adaptability. Key pathways such as mRNA editing and formation of the editosome indicate that ruxolitinib may influence RNA editing mechanisms, which could impact the solubility and translation of oncogenes. Pathways related to rRNA processing in the nucleus and cytosol and the broader Metabolism of RNA indicate potential disruption in ribosomal RNA biogenesis, an essential process for cancer cell growth and proliferation [52]. These intersecting pathways underscore ruxolitinib's many-sided approach to AML treatment, where disruption of both RNA processing and protein synthesis pathways limits cancer cell adaptability and growth [53]. Comparing intersectional targets with those unique to lysate and living cell samples, it appears that ruxolitinib exerts its effects by not only disrupting core protein synthesis and RNA regulation in the cytosol (lysate sample targets) but also by impacting broader cellular machinery like epigenetic and

transcriptional regulation (living cell sample targets), ultimately converging on mechanisms critical to cancer cell survival and metabolic flexibility.

In the sample treated with ulixertinib, 602 proteins displayed altered solubility in lysate samples and 295 in living cell samples, with 22 proteins overlapping between the two conditions (**Fig. 4, Supplementary File 1**). The pathway enrichment analysis reveals ulixertinib primarily targeted pathways involved in RNA processing, DNA repair, and metal ion homeostasis. Notably, the Metabolism of the RNA pathway was significantly enriched, suggesting that ulixertinib may disrupt RNA metabolic processes essential for cancer cell growth and proliferation. Enrichment of the mRNA Splicing - Major Pathway and Processing of Capped Intron-Containing Pre-mRNA indicates that ulixertinib may influence splicing mechanisms, potentially affecting the regulation of oncogenic transcripts [54]. Together, these results suggest that ulixertinib's effects in AML involve modulating RNA metabolism, splicing, metal ion response, and genomic repair mechanisms.

In living cell samples, ulixertinib targets additional pathways that highlight broader regulatory roles in DNA maintenance, chromatin modification, and cellular senescence. Key pathways including HDACs Deacetylate Histones, RHO GTPases Activate PKNs, and RNA Polymerase I Promoter Opening, suggesting that ulixertinib may influence histone modification and RNA transcription processes pivotal to AML progression [55]. DNA methylation and base excision repair pathways are also significantly enriched, underscoring ulixertinib's impact on DNA stability, which is crucial in counteracting the genomic instability characteristic of AML. This enrichment of epigenetic pathways suggests that ulixertinib might hinder AML cell growth by altering transcriptional landscapes and promoting DNA repair deficiencies, which could enhance its efficacy in AML therapy.

In both living cells and lysate samples, ulixertinib demonstrated consistent targeting of pathways associated with RNA processing, DNA repair, and immune modulation. The drug's influence on RNA processing is reinforced by pathways such as mRNA splicing and RNA Polymerase II transcription, suggesting interference with gene expression and protein synthesis. Enrichment of DNA repair pathways, including nucleotide excision repair and DNA double-strand break repair, implies that ulixertinib may sensitize cancer cells to DNA damage, thus enhancing susceptibility to apoptosis. Furthermore, enrichment of immune-related pathways, including cytokine and Toll-like receptor signaling, suggests potential immunomodulatory effects, contributing to its therapeutic impact.

Overall, a comparison between ulixertinib's effects in lysate and living cell samples highlights a miscellaneous mechanism of action. Lysate-specific pathways emphasize disruptions in RNA processing and metal ion responses, potentially impairing basic cellular metabolism[56,57]. In contrast, living cell-specific pathways reveal broader influences on epigenetic regulation and DNA repair, hinting at ulixertinib's capacity to impact higher-order transcriptional and genomic integrity processes in AML cells. This combination of targeting core cellular functions in lysate samples and regulatory pathways in living cell samples underscores ulixertinib's complex therapeutic profile in AML, disrupting essential mechanisms of cancer cell survival and adaptability.

Mechanistic Insights into "AND" and "OR" Gate Targeting Patterns

In the comparative analysis of proteins with significant solubility shifts in CoPISA experiments from the LY3009120 and sapanisertib combination, distinct pathway enrichment

patterns are observed between the lysate and living cell samples **(Supplementary File 1)**. Key enriched pathways in "AND" gate in lysate sample include costimulation by the CD28 family, which suggest that the combination influences immune cell activation, potentially enhancing anti-tumor immunity within the tumor microenvironment **(Fig. 8A)**. Additionally, pathways related to rRNA processing, Major pathway of rRNA processing in the nucleolus and cytosol, and rRNA processing in the nucleus and cytosol are significantly enriched, indicating that this drug combination may disrupt ribosomal biogenesis, a process crucial for supporting rapid protein synthesis in proliferating AML cells [58]. The involvement of Signaling by CSF1 (M-CSF) in myeloid cells highlights potential effects on myeloid cell signaling pathways, which may contribute to altering the AML cell environment and promoting cell differentiation or apoptosis [59]. Additionally, enriched pathways related to Mitochondrial translation initiation, Mitochondrial translation elongation, and Mitochondrial translation termination suggest that the drug combination could interfere with mitochondrial protein synthesis, which may affect cellular energy production and apoptosis regulation, further weakening AML cell survival mechanisms. These results collectively indicate that the combinations specific targets of LS may exert a complementary therapeutic effect by modulating immune pathways [60], impairing ribosomal and mitochondrial function [61], and targeting myeloid-specific signaling, making this combination a promising strategy for AML treatment.

In the living cells treated with the LS combination, there is a significant enrichment of pathways critical for cancer cell regulation and survival. Notably, Metalloprotease DUBs and RMTs methylate histone arginine pathways indicate profound impacts on protein solubility and epigenetic modifications essential for cancer progression [62]. The enrichment of Pre-NOTCH Expression and Processing and HATs acetylate histones underscore the combination's role in modulating transcription factors and chromatin structure that are crucial in cell differentiation and proliferation [63]. Pathways such as Formation of the beta-catenin transactivating complex and B-WICH complex positively regulates rRNA expression also highlight the treatment's ability to influence Wnt signaling and ribosomal biogenesis—both key to maintaining the malignant phenotype. Furthermore, the enrichment of pathways such as PKN1 activation drives AR-regulated transcription of KLK2/3 highlights how the combination influences androgen receptor signaling [64]. This intricate interplay of pathways significantly enriched in the living cells paints a detailed picture of how LY3009120 and sapanisertib disrupt multiple core cellular processes, offering a robust therapeutic strategy against AMLt.

The combination of LS demonstrates a synergistic effect on both lysate and living cell samples, targeting distinct yet interconnected cellular processes. Living cell samples exhibiting enhanced epigenetic and transcription regulation suggest a direct interference with cancer cell's genetic machinery, aiming to alter the fundamental cellular properties that sustain malignant phenotypes. In contrast, the lysate samples, displaying pathways involved in protein synthesis and immune modulation, suggest an external modulation of the tumor microenvironment and metabolic pathways, which could indirectly lead to tumor regression or sensitize the cells to other treatments.

The "OR" gate analysis of proteins targeted by either LY3009120,sapanisertib or LS in the lysate sample reveals a significant effect on key metabolic pathways that influence cell growth and survival via modulation of growth factor signaling. Other critically enriched pathways such as Post-translational protein phosphorylation could indicate the extensive modification of protein functions, which could impact multiple signaling pathways critical for cancer progression and

response to therapy [65]. The Digestion of dietary carbohydrate and Non-integrin membrane-ECM pathways interactions, respectively, highlight the treatment's broader implications on cellular metabolism and interaction with the extracellular matrix, crucial for cancer cells' invasive and metastatic properties [66]. These shared pathways underscore a multifaceted disruption of cellular homeostasis and signaling by the drug treatments, providing a potential therapeutic advantage by simultaneously targeting various aspects of cancer cell biology that are pivotal for their proliferation and survival.

Within the same gate in living cells treatments influenced key signaling pathways like p130Cas linkage to MAPK signaling for integrins and GRB2, underline the role of integrin-mediated signaling in cellular adhesion and migration processes that are crucial for tumor metastasis and invasion [67]. The activation pathways for MAPK via different mutants of BRAF and RAF1, as evidenced by Signaling by high-kinase activity BRAF mutants and Signaling by RAF1 mutants, indicate the profound influence these drugs have on modulating key cancer growth and survival pathways. The convergence on MAPK signaling, integral to cell proliferation and differentiation, underscores the potential of these drugs to interfere with signaling cascades that are often deregulated in cancers [68]. Additionally, pathways like Integrin signaling and Platelet Aggregation are indicative of the drugs' impact on not only the tumor cells but also the tumor microenvironment, affecting processes such as angiogenesis and thrombosis, which are vital for tumor sustenance and spread [69]. Moreover, Senescence-Associated Secretory Phenotype (SASP) being targeted suggests a strategy to exploit cellular aging mechanisms to suppress tumor growth and possibly induce a senescence-associated growth arrest [70]. The broad effect on these pathways demonstrates the potential of LS to not only target cancer cell proliferation directly but also modulates the intracellular and extracellular communication pathways that support the malignant phenotype.

The enriched pathways from the RU-treated samples in lysate condition offer insights into their potential mechanisms in treating AML. Notably, pathways such as Signaling by TGF-beta Receptor Complex and TGF-beta receptor signaling activates SMADs emphasize the drugs' impact on crucial signaling cascades that regulate cell growth and differentiation. These pathways are integral to cellular homeostasis and are often dysregulated in cancer, indicating that the drug combination may restore normal signaling or counteract malignant signaling in AML [71]. The targeting of transcriptional regulation by NPAS4 and the AP-2 family of transcription factors also highlights the influence on gene expression linked to cellular stress responses and apoptosis. These transcription factors play pivotal roles in responding to cellular environment changes, which can dictate cell survival or death pathways that are particularly relevant in cancer therapy [72]. Additionally, pathways like RUNX1 regulates transcription of genes involved in interleukin signaling and Cyclin D associated events in G1 suggest that the combination therapy may also be affecting the cell cycle and immune-related responses, which are critical in the proliferation and survival of leukemia cells [73]. These findings suggest that RU combination disrupt key regulatory networks essential for AML cell maintenance and proliferation. By modulating growth factor signaling, gene transcription, and cell cycle progression, this combination therapy potentially offers a multifaceted approach to impairing AML cell growth and enhancing the efficacy of existing therapeutic regimes.

The living cells treated with the combination of RU highlight several significantly enriched pathways that illustrate how this therapeutic may impact AML. Pathways such as Interleukin-1 signaling and Interleukin-1 family signaling, suggest a profound effect on inflammation pathways

that are often linked with the cancer inflammation microenvironment. These pathways are critical as they can influence tumor progression and response to therapy by modulating the immune landscape within the tumor microenvironment [74]. Moreover, pathways like mRNA decay by 5' to 3' exoribonuclease indicate an impact on gene expression regulation, highlighting the treatment's potential to affect mRNA solubility and thereby control the translation of genes involved in cancer cell proliferation and survival [75]. Additionally, Signaling by TGF-beta Receptor Complex underscores a direct involvement in growth factor signaling pathways that are crucial for cell differentiation and cancer cell migration. The inclusion of pathways such as Biosynthesis of aspirin-triggered D-series resolvins and Biosynthesis of E-series 18(R)-resolvins also points to the drugs' potential roles in resolving inflammation and promoting a return to tissue homeostasis, which can be particularly beneficial in reducing tumor-promoting inflammation in AML [76]. These pathways emphasize the potential of RU combination to modulate not only key signaling pathways directly involved in cancer progression but also those that regulate the immune environment and inflammatory responses, supporting their role in comprehensive cancer therapy strategies that target multiple facets of cancer biology.

The comparison of pathways affected in living and lysate cells in RU combination treatment, reveals that while both sample types are affected by the drug combination, the living sample's response involves a broader modulation of the immune environment, which could lead to a more systemic impact on tumor dynamics. In contrast, the lysate sample focuses on disrupting fundamental cellular signaling pathways that can lead to inhibited tumor growth and induced apoptosis. This dual approach—targeting both the tumor cells directly and the tumor microenvironment—might be why combinations of drugs like ruxolitinib and ulixertinib can be particularly effective in treating complex malignancies like AML. Each approach leverages different aspects of cancer biology: one mitigating the supportive tumor microenvironment and the other halting the cellular mechanisms of tumor progression.

The analysis of proteins targeted within the “OR” gate of either ruxolitinib, ulixertinib, or RU in lysate samples reveals significant enrichment in pathways associated with cellular translation and metabolism, presenting a comprehensive disruption of critical cellular processes essential for cancer cell viability **(Fig. 10)**. Notably, the most significantly impacted pathway, Translation, underscores the profound effect the drug combination has on the general protein synthesis machinery, which is a cornerstone for rapid cancer cell proliferation and survival [77]. Furthermore, specific enrichment in pathways such as Peptide chain elongation and Eukaryotic Translation Termination, highlights the drugs' capacity to interfere directly with the synthesis of new proteins, which could lead to halted growth or apoptosis of cancer cells [78]. The extensive impact on rRNA processing pathways, with Selenoamino acid metabolism and Major pathway of rRNA processing in the nucleolus and cytosol, indicates a targeted disruption in ribosome biogenesis—a process crucial for cell growth and proliferation. Such disruptions are particularly detrimental to cancer cells, which require robust protein synthesis machinery to maintain their growth rates. Collectively, these pathways' modulation by ruxolitinib and ulixertinib highlights a multifaceted attack on the protein synthesis and growth regulation mechanisms within AML cells. This broad spectrum of interference in fundamental cellular processes not only undermines the cancer cells' ability to proliferate and survive but also enhances the potential of these drugs to act synergistically with existing therapies to improve outcomes in AML treatment.

The analysis of protein targets affected by ruxolitinib, ulixertinib, or their combination (RU) in “OR” gate in living cells, reveals a profound impact on several essential biological processes with high significance. Key pathways such as Packaging Of Telomere Ends and Cleavage of the damaged purine, indicate a robust influence on DNA integrity and repair mechanisms. These pathways are critical in maintaining genomic solubility, a pivotal factor in cancer progression and the response to therapy [79]. The enrichment in HDACs deacetylate histones and RNA Polymerase I Promoter Opening pathways suggests that the drugs extensively modulates chromatin architecture and transcriptional regulation. Such modulation can alter the expression patterns of genes critical for cell cycle control and apoptosis, potentially reinstating controlled growth and cell death in AML cells where these processes are typically dysregulated. Furthermore, the impact on DNA methylation and recognition and repair pathways associated with damaged DNA highlights the drugs' roles in influencing epigenetic modifications and correcting DNA damage response mechanisms. These are vital for correcting the proliferative nature of AML and other cancers, where faulty DNA repair mechanisms often contribute to malignancy and resistance to therapy. Altogether, these findings underscore the potential of RU combination in targeting and modulating multiple molecular pathways that are crucial for the survival and proliferation of cancer cells. By impacting telomere dynamics, histone modification, DNA repair, and transcription regulation, this combination therapy could provide a multifaceted approach to cancer treatment, enhancing the effectiveness of existing therapies and potentially leading to better clinical outcomes in AML treatment. The broad impact across these pathways not only demonstrates the potential for direct anticancer effects but also suggests a role in sensitizing cancer cells to other therapeutic agents by undermining cellular resistance mechanisms.

In the detailed comparative analysis of the "AND" and "OR" gate targeting patterns in the samples treated with LY3009120,ruxolitinib, or RU distinct pathways emerge that are exclusively influenced under the "AND" gate conditions, both in the lysate and living samples. Specifically, in the lysate samples, pathways such as Co-stimulation by the CD28 family and Major pathway of rRNA processing in the nucleolus and cytosol are uniquely affected, indicating a precise modulation of immune cell activation and ribosomal biogenesis that is not observed in the "OR" gate configurations. Similarly, in the living samples, pathways like GRB2 events in ERBB2 signaling and Signaling by high-kinase activity BRAF mutants are specifically enriched, highlighting the targeted impact on key cancer progression mechanisms. These unique pathway enrichments under the "AND" gate conditions emphasize the potential of conjunctional inhibition, where the cooperative interaction between drugs results in specific biological effects that are not attainable through the individual or overlapping actions of the drugs. Such insights not only validate the concept of conjunctional inhibition but also underscore its importance in developing more effective combination therapies that can precisely target and disrupt complex disease pathways, offering a more refined and potentially more effective approach to cancer treatment. This nuanced understanding of drug interactions enhances our ability to tailor therapeutic strategies that leverage the full potential of drug combinations, potentially leading to improved treatment outcomes in AML and other complex diseases.

For the ruxolitinib, ulixertinib, and RU treatments, the "AND" and "OR" gate analyses reveal distinct patterns in biological pathway targeting that elucidate the mechanisms of conjunctional inhibition, particularly in the lysate sample. The "AND" gate analysis identified unique pathways such as Alanine metabolism and Defective Galactose-1-phosphate uridylyltransferase (GALT) can

cause galactosemia (GALCT), which were not observed under the "OR" gate conditions. This suggests a complex interplay where both ruxolitinib and ulixertinib are required simultaneously to exert effects on these metabolic processes. Similarly, Downregulation of TGF-beta receptor signaling and Transcriptional Regulation by NPAS4 in the "AND" gate further underscore the drugs' cooperative modulation of critical pathways that regulate cell growth and apoptosis, highlighting their potential to intricately modulate signaling pathways that are crucial for AML progression. Conversely, the "OR" gate, demonstrating overlapping effects from either drug alone or in combination, did not show significant changes in these pathways, indicating that certain critical cellular processes are uniquely influenced only under the concurrent presence of both drugs. Such findings stress the strategic importance of conjunctional inhibition within combination therapies, where the interaction of drugs can lead to unique therapeutic effects not achievable by either agent alone, offering a robust strategy to combat the multifaceted nature of AML.

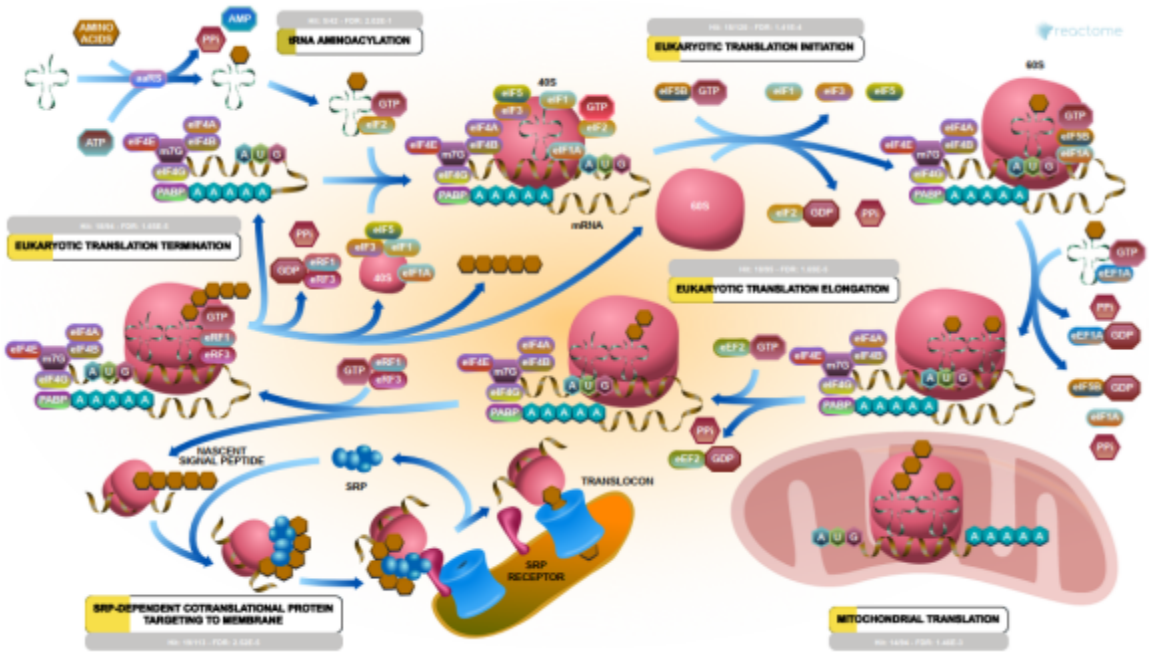

Figure 11. Pathway Illustrations of Cellular Processes Affected by ruxolitinib and ulixertinib in AML Treatment. Translation in RU lysate: This panel shows the extensive impact of ruxolitinib and ulixertinib on protein synthesis processes in lysate samples of AML cells. Exported from the Reactome database.

Discussion

Combination therapy has been a mainstay in cancer treatment, particularly for aggressive malignancies like AML, due to its potential to overcome resistance and improve patient outcomes[80]. Initially, the goal was to reduce the likelihood of resistance by using multiple agents with distinct mechanisms of action, aiming to target cancer cells through various pathways simultaneously [81]. However, the selection of effective drug combinations has been challenging due to the genetic and epigenetic heterogeneity of AML, which results in varied responses to treatment across different patients[82]. Additionally, the high toxicity associated with multi-drug regimens limits their utility, often causing significant side effects that restrict dosage levels and treatment duration [83]. This complexity has driven a shift in the approach to combination therapy, with a focus on understanding the molecular basis of drug interactions to design rational, synergistic drug combinations that maximize efficacy while minimizing toxicity [18]. While recent approaches have focused on understanding the additive or synergistic effects of individual drugs[80], our study introduces a novel concept termed "conjunctional inhibition". This concept suggests that the combined action of drugs distinctively alters certain biological responses compared to individual drugs.

In this study, we introduced the CoPISA methodology to evaluate the effects of two recently proposed combinatorial treatments for AML: LY3009120-sapanisertib and ruxolitinib-ulixertinib [18]. CoPISA workflow captures drug-induced changes in protein solubility specifically arising from the combined action of drugs, offering insights into mechanisms that single-drug treatments cannot achieve. The approach allowed us to identify both primary and secondary protein targets, revealing cellular responses linked to combination therapies. These findings suggest that the interactions between the two drugs in each pair are not merely additive but involve more complex cooperative mechanisms. This novel concept reflects a situation where the concurrent action of two agents produces distinct biological effects unattainable by individual drugs, indicating a deeper level of interaction between the two drugs' targets and signaling pathways.

We also provide valuable insights into the molecular mechanisms underlying the therapeutic effects of these drug combinations. By comparing the identified proteins with significant solubility shifts with known drug targets, we were able to validate the functional significance of the proteins identified in our study. These findings offer potential avenues for further investigation and the development of novel therapeutic strategies.

In conclusion, our study introduces a novel approach for understanding the mechanisms of combination therapy and provides valuable insights into the potential of conjunctional inhibition as a therapeutic strategy for AML. By leveraging the power of CoPISA and advanced proteomic analysis, we have identified key molecular targets and pathways that may be modulated by combination therapies. These findings offer promising avenues for the development of more effective and personalized treatments for AML patients.

Material and Methods

Ab Initio Simulation

The simulation of sigmoidal curves of 10000 hypothetical proteins was carried out using R and melting temperatures T_m selected randomly in the range from 48 to 56 °C. N_t = 15 temperature points between 45 and 59 °C with a 1 °C step were chosen. Sigmoidal melting curves were simulated by calculating the relative intensity $I(T)$ for a given temperature T as $Intensity(T)_{control} = 0.5\, erf[(T_m - T)/sqrt(T_m)/2$ where erf is the error function, and $sqrt$ is the square root function. Similarly, sigmoidal melting curves for treated samples was simulated as $Intensity(T)_{treated} = 0.5\, erf[(T_m + \Delta T_m - T)/sqrt(T_m + \Delta T_m)/2$. ΔT_m were simulated as random values in the range between $-$ 3°C and $+$ 3°C. The sum of measured signal for control and treated samples calculated as $S_m = \sum_{T=1}^{15} Intensity(T)$, for all temperature points. The treatment here was simulated for two hypothetical drugs to calculate S_m values, i.e., $S_m^{control}$, S_m^1 and S_m^2. In the next step, we calculated the two ΔS_m for both hypothetical drugs, i.e., ΔS_m^1 and ΔS_m^2 in 10,000 proteins to depict versus each other.

Cell culture

MOLM-13, MOLM-16, SKM and NOMO-1 cells were obtained from Deutsche Sammlung von Mikroorganismen und Zellkulturen (DSMZ, Germany) and cultured in RPMI-1640 medium (Gibco, Thermo Fisher Scientific, USA) supplemented with 10–20% fetal bovine serum (FBS) (Gibco, Thermo Fisher Scientific), 2 mM L-glutamine (Lonza), and 100 units/mL penicillin/streptomycin (Gibco, Thermo Fisher Scientific), at 37°C and 5% CO2. Cells were harvested and centrifuged at 400 g for 4 min.

Cell lysate based CoPISA

Cells were cultured until they reached the desired density of 2×10^6 cells per treatment with seven different treatment groups for each cell line, performed in triplicate. A 24 ml volume of cell culture was pelleted by centrifugation at 600g for 5 minutes, followed by two washes with phosphate-buffered saline (PBS). After a final pelleting, cells were resuspended in PBS (GIBCO) supplemented with protease inhibitors (Roche, Switzerland). The cell mixture was lysed through 4 cycles of freezing in liquid N2 and then thawing at 35 °C, at the final step cells were cleared by centrifugation at 10,000 g for 10 min at 4 °C. Samples were then treated with single or combination drug regimens at the following concentrations: LY3009120 500 nm, sapanisertib 500 nM, ruxolitinib 3uM, ulixertinib 3uM, for 15 min at room temperature, After treatment, the samples were aliquoted into 12 equal volumes for subsequent heat treatments. Each aliquot was subjected to a 3-minute heat treatment at temperatures ranging from 48°C to 59°C in 1°C intervals using a thermocycler (Applied Biosystems Veriti). After equilibrating at room temperature for 3 min,

samples from different temperatures for each drug treatment were pooled and subjected to ultracentrifugation at 100,000g for 20 minutes at 4°C (Beckman Coulter Optima Max-XP). The soluble proteins from the supernatant were collected for further analysis.

Living cell-based CoPISA

Cells (2 × 106 cells per condition) were treated with a single or combination drug with concentrations mentioned, in 6-well plates and incubated at 37°C with 5% CO_2 for 60 min. Following treatment, the cells were washed twice with PBS and resuspended in 320 µL of PBS supplemented with a protease inhibitor. An equal volume of each sample was transferred to the PCR plate and was heated for 3 min at the same temperatures used in the lysate-based protocol. The samples were allowed to cool down at room temperature for 3 min and then applied for four cycles of freezing cells in liquid N2 and thawing at 35 °C. After pooling the samples from different temperature points for each treatment, the soluble proteins were isolated via ultracentrifugation 100,000g for 20 min at 4°C. At this point, samples can be flash frozen and stored at -80°C for future analysis.

Proteomics Sample Processing

Protein concentration was measured using the PierceBCA Protein Assay Kit (Thermo), and the volume corresponding to 27 µg of protein was transferred from each sample to prepared filter tubes (Amicon Ultra-0.5 mL Centrifugal Filters 10KD). The volume of each sample was adjusted to an equal level using 20 mM 4-(2-hydroxyethyl)-1-piperazinepropanesulfonic acid (EPPS) buffer, then was reduced in 10 mM dithiothreitol (55 °C, 30 min) and alkylated in 50 mM iodoacetamide (25 °C, 60 min in darkness). After reduction and alkylation, samples were centrifuged for 20 min, 14000g, followed by two washes. EPPS buffer was then added to the Amicon filter tubes containing samples. Proteins were digested overnight at 37°C with vigorous shaking by trypsin at a ratio of 1:50. The resulting peptides were collected by centrifugation and rinsing the filter tubes with EPPS. Prior to labeling, equal amounts of each sample from the different treatment groups were mixed for separate labeling. A total of 25 µg from each sample was labeled using tandem mass tags (TMT) according to the manufacturer's protocol (Thermo Fisher Scientific). Three technical replicates for each treatment (drug A, Drug B, Drug AB and control) along with one mixed sample of each condition were pooled together resulting in a final mixture of 325 µg from 13 samples.

Peptide fractionation and LC MS/MS analysis

TMT-labeled peptides were fractionated by high-pH reversed phase separation using a XBridge Peptide BEH C18 column (3.5 µm, 130 Å, 1 mm x 150 mm, Waters) on an Ultimate 3000 system (Thermo Scientific). Peptides were loaded on column in solution A and the system was run at a flow of 42 µl/min. The following gradient was used for peptide separation: from 2% B to 15% B over 3 min to 45% B over 59 min to 80% B over 3 min followed by 9 min at 80% B then back to 2% B over 1 min followed by 15 min at 2% B. Solution A was 20 mM ammonium formate in water, pH 10 and SolutionB was 20 mM ammonium formate in 90% acetonitrile, pH 10. Elution of peptides

was monitored with a UV detector (205 nm, 214 nm) and a total of 36 fractions were collected, pooled into 12 fractions using a post-concatenation strategy as previously described (Wang et al., 2011) and dried under vacuum.

Dried peptides were resuspended in 0.1% aqueous formic acid and subjected to LC–MS/MS analysis using an Orbitrap Eclipse Tribrid Mass Spectrometer fitted with a Ultimate 3000 nano system and a FAIMS Pro interface (all Thermo Fisher Scientific) and a custom-made column heater set to 60°C. Peptides were resolved using a RP-HPLC column (75 µm × 30 cm) packed in-house with C18 resin (ReproSil-Pur C18–AQ, 1.9 µm resin; Dr. Maisch GmbH) at a flow rate of 0.3 µl/min. The following gradient was used for peptide separation: from 2% B to 12% B over 5 min to 30% B over 70 min to 50% B over 15 min to 95% B over 2 min followed by 18 min at 95% B then back to 2% B over 2 min followed by 18 min at 2% B. Solution A was 0.1% formic acid in water and Solution B was 80% acetonitrile, 0.1% formic acid in water.

The mass spectrometer was operated in DDA mode with a cycle time of 3 s between master scans. Throughout each acquisition, the FAIMS Pro interface switched between CVs of −40 V and −70 V with cycle times of 1.5 s and 1.5 s, respectively. MS1 spectra were acquired in the Orbitrap at a resolution of 120,000 and a scan range of 400 to 1600 m/z, AGC target set to "Standard" and maximum injection time set to "Auto". Precursors were filtered with precursor selection range set to 400–1600 m/z, monoisotopic peak determination set to "Peptide", charge state set to 2 to 6, a dynamic exclusion of 45 s, a precursor fit of 50% in a window of 0.7 m/z and an intensity threshold of 5e3. Precursors selected for MS2 analysis were isolated in the quadrupole with a 0.7 m/z window and collected for a maximum injection time of 35 ms with AGC target set to "Standard". Fragmentation was performed with a CID collision energy of 30% and MS2 spectra were acquired in the IT at scan rate "Turbo".

MS2 spectra were subjected to RTS using a human database containing 20362 entries downloaded from Uniprot on 20200417 using the following settings: enzyme was set to "Trypsin", TMTpro16plex (K and N-term) and Carbamidomethyl (C) were set as fixed modification, Oxidation (M) was set as variable modification, maximum missed cleavages were set to 1 and maximum variable modifications to 2. Maximum search time was set to 100 ms, the scoring threshold was set to 1.4 XCorr, 0.1 dCn, 10 ppm precursor tolerance, charge state 2 and "TMT SPS MS3 Mode" was enabled. Subsequently, spectra were filtered with a precursor selection range filter of 400–1600 m/z, precursor ion exclusion set to 25 ppm low and 25 ppm high and isobaric tag loss exclusion set to "TMTpro". MS/MS product ions of precursors identified via RTS were isolated for an MS3 scan using the quadrupole with a 2 m/z window and ions were collected for a maximum injection time of 200 ms with a normalized AGC target set to 200%. SPS was activated and the number of SPS precursors was set to 10. Isolated fragments were fragmented with normalized HCD collision energy set to 55% and MS3 spectra were acquired in the Orbitrap with a resolution of 50,000 and a scan range of 100 to 500 m/z.

The acquired raw-files were analysed using the SpectroMine software (v3.2, Biognosis AG). Spectra were searched against a human database consisting of 20360 protein sequences (downloaded from Uniprot on 20220222). Standard Pulsar search settings for TMT 16 pro ("TMTpro_Quantification") were used as follows. In the Peptides tab, Enzyme / Cleavage was set to Trypsin/P, Digest Type was set to Specific, Max Peptide Length was set to 52, Min Peptide Length was set to 7, 2 Missed cleavages were allowed and Toggle N-terminal M was activated. In the

Labeling tab, Channels 1, 2 and 3 were unchecked. In the modifications tab, Do Modification Localization was enabled, Max Variable Modifications was set to 5, Carbamidomethyl (C), TMTpro_Lys and TMTpro_Nter were set as fixed modifications, Acetyl (Protein N-term) and Oxidation (M) were set as variable modifications. In the MS1 tab, Number of searches was set to 1, in the MS2 tab Ion Types was set to b and y and MS2 DeMultiplexing was set to Automatic and in the MS3 tab Use MS3 was enabled. In the Speed-Up tab, Calibration Search Max Variable Modifications was set to 1, Specific was enabled and MS2 Index was set to Automatic use. In the identification tab, PSM, Peptide and Protein Group FDR were set to 0.01 and Exclude Single Hit Proteins was unchecked. Resulting identifications and corresponding quantitative values were exported on the PSM level using the "Export Report" function.

LC-MS Analysis of Drug Combinations

Ten picomoles from each drug, separately or combined were injected into LCMS (Eksigent Ekspert 400 coupled to TripleTOF 6600 (Sciex, USA)). These analytes were separated using a linear gradient of 15 min comprising 8 min from 3 % to 35 % of solution B (0.1 % formic acid / acetonitrile) and 2 min to 90 % of solution B on a reverse phase C4 column(0.3 x 20mm, Phenomenex, USA). The solution A was 0.1 % formic acid and the flow rate was at 5ul/min. The mass spectrometer was set in TOF MS mode with the following parameters: Ion spray voltage was at 5500 volts, ion source and curtain gases 10 and 30 liter per minute respectively. TOF MS was acquired from m/z 200 to 1500. Following LC-MS acquisition, raw files were analyzed by PeakView® software, version 2.2 (Sciex). Drug ions were extracted using their corresponding m/z +/- 0.5 Da.

Statistical Analysis

Proteomics data were obtained from primary Peptide Spectrum Match (PSM) reports, providing raw intensity values of peptides identified across experimental conditions. Invalid or missing treatments were excluded, and intensity values were normalized to account for differences in protein abundance across samples. A pooled control sample was used for further normalization, and protein intensities were averaged across replicates to create matrices for each treatment condition.

Linear modeling with empirical Bayes adjustments was applied for statistical analysis. Comparisons were made between control (C) and drug treatment conditions (R, U, RU, L, S, LS). Contrast matrices were defined to account for single and combination drug effects, with significance thresholds set at p-value < 0.05. Volcano plots were generated for each treatment comparison to visualize significantly upregulated and downregulated proteins based on logFC and p-values. Fold change plots comparing each combination of treatments (comb vs drug1, comb vs drug2, and drug1 vs drug2) were generated, with primary plots displaying fold changes across the full dataset range and inset plots highlighting a focused subset of the most significant proteins based on p-values.

Due to the complexity of comparing single drugs and combinations in the CoPISA method, an a priori understanding of the error distribution was unavailable, preventing direct multiple hypothesis correction. To address this, we tested our candidate selection procedure and estimated the false discovery rate (FDR) for proteins with significant solubility shifts. This involved permuting the protein Sm values across replicates within the dataset to generate randomized datasets[84–86]. The

same selection criteria were applied to these permuted datasets as to the original data, enabling us to evaluate the robustness of our approach and ensure confidence in the identified candidates.

Pathway Enrichment Analysis

The exclusive proteins with significant solubility shifts in each treatment were subjected to pathway enrichment analysis using the Ingenuity Canonical Pathways database and Reactome server. For Reactome pathway analysis, proteins were uploaded with their respective identifiers, and the analysis was performed using the default Reactome parameters unless specified otherwise. To focus on biological processes with the most significant pathways the Benjamini-Hochberg correction was applied to calculate false discovery rate (FDR)-adjusted p-values. Pathways with an FDR-adjusted p-value ≤ 0.05 were considered significantly enriched.. Pathways shared between the two conditions were highlighted, providing insight into common responses to treatment.

Contributions

M.J. conceived the study and designed the research questions. M.J. and A.A. provided scientific direction, supervised the project, and contributed to the manuscript preparation. E.G. led the experimental analyses and data interpretation, while E.Z. led the computational analyses and data visualization. U.V. participated in proteomics data analysis, and D.R. conducted the proteomics mass spectrometry experiments and data analysis. J.J.M. assisted with protein extraction and interpretation of signaling networks. R.S. and M.B. contributed to small-molecule mass spectrometry analysis. M.W. supported the interpretation of findings and the validation experimental design. C.A.H. provided cell lines and contributed to interpretation of findings.

Data availablity

Proteomic data have been deposited to the ProteomeXchange Consortium (https://www.proteomexchange.org/) via the MassIVE partner repository with MassIVE data set identifier MSV000096500 and ProteomeXchange identifier PXD058177 .

Supplementary

Supplementary file 1: Excel file containing pathway enrichment analysis results for Reactome database, organized into 16 sheets. Each sheet presents the enriched pathways identified for treatments involving a single drug and drug combinations under two experimental conditions: living cells and lysate extract. Analyses are separated for LS and RU combinations, providing detailed pathway insights for both treatments. Each sheet contains pathway names, reaction identifiers, statistical values, and etc supporting comprehensive comparison across conditions and combinations.

Acknowledgements:

The authors acknowledge Meilahti Clinical Proteomics Core Facility for Mass Spec. sample analysis, (supported by HiLIFE and Biocenter Finland).

References

1. Döhner, K., Paschka, P. & Döhner, H. [Acute myeloid leukemia]. *Internist* **56**, 354–363 (2015).
2. Cherry, E. M. *et al.* Venetoclax and azacitidine compared with induction chemotherapy for newly diagnosed patients with acute myeloid leukemia. *Blood Adv.* **5**, 5565–5573 (2021).
3. Karol, S. E. *et al.* Venetoclax in combination with cytarabine with or without idarubicin in children with relapsed or refractory acute myeloid leukaemia: a phase 1, dose-escalation study. *Lancet Oncol.* **21**, 551–560 (2020).
4. Mason-Osann, E., Pomeroy, A. E., Palmer, A. C. & Mettetal, J. T. Synergistic Drug Combinations Promote the Development of Resistance in Acute Myeloid Leukemia. *Blood Cancer Discov* **5**, 95–105 (2024).
5. Chen, S. *et al.* Combining kinase inhibitors for optimally co-targeting cancer and drug escape by exploitation of drug target promiscuities. *Drug Dev. Res.* **82**, 133–142 (2021).
6. Tang, K., Schuh, A. C. & Yee, K. W. 3+7 Combined Chemotherapy for Acute Myeloid Leukemia: Is It Time to Say Goodbye? *Curr. Oncol. Rep.* **23**, 120 (2021).
7. Wang, J., Tomlinson, B. & Lazarus, H. M. Update on Small Molecule Targeted Therapies for Acute Myeloid Leukemia. *Curr. Treat. Options Oncol.* **24**, 770–801 (2023).
8. Atallah, E. L. Why isn't there a one-size-fits-all approach for relapsed/refractory acute myeloid leukemia? Insights into different variables for decision-making. *Best Pract. Res. Clin. Haematol.* **34**, 101240 (2021).
9. Nair, R., Salinas-Illarena, A. & Baldauf, H.-M. New strategies to treat AML: novel insights into AML survival pathways and combination therapies. *Leukemia* **35**, 299–311 (2021).
10. Ianevski, A. *et al.* Single-cell transcriptomes identify patient-tailored therapies for selective co-inhibition of cancer clones. *Nat. Commun.* **15**, 8579 (2024).
11. Mishra, R., Zokaei Nikoo, M., Veeraballi, S. & Singh, A. Venetoclax and hypomethylating agent

combination in myeloid malignancies: Mechanisms of synergy and challenges of resistance. *Int. J. Mol. Sci.* **25**, (2023).

12. Mateus, A., Määttä, T. A. & Savitski, M. M. Thermal proteome profiling: unbiased assessment of protein state through heat-induced stability changes. *Proteome Sci.* **15**, 13 (2016).
13. Zangene, E., Gholizadeh, E. & Jafari, M. DORSSAA: Drug-target interactOmics Resource based on Stability/Solubility Alteration Assay. *bioRxiv* (2023) doi:10.1101/2023.12.29.573639.
14. Kaur, U. *et al.* Proteome-Wide Structural Biology: An Emerging Field for the Structural Analysis of Proteins on the Proteomic Scale. *J. Proteome Res.* **17**, 3614–3627 (2018).
15. Gaetani, M. *et al.* Proteome Integral Solubility Alteration: A High-Throughput Proteomics Assay for Target Deconvolution. *J. Proteome Res.* **18**, 4027–4037 (2019).
16. Saei, A. A. *et al.* Multifaceted Proteome Analysis at Solubility, Redox, and Expression Dimensions for Target Identification. *Adv Sci (Weinh)* **11**, e2401502 (2024).
17. Van Vranken, J. G. *et al.* Large-scale characterization of drug mechanism of action using proteome-wide thermal shift assays. *bioRxiv* (2024) doi:10.1101/2024.01.26.577428.
18. Mirzaie, M. *et al.* Designing patient-oriented combination therapies for acute myeloid leukemia based on efficacy/toxicity integration and bipartite network modeling. *Oncogenesis* **13**, 11 (2024).
19. Franken, H. *et al.* Thermal proteome profiling for unbiased identification of direct and indirect drug targets using multiplexed quantitative mass spectrometry. *Nat. Protoc.* **10**, 1567–1593 (2015).
20. Savitski, M. M. *et al.* Tracking cancer drugs in living cells by thermal profiling of the proteome. *Science* **346**, 1255784 (2014).
21. Jafari, M., Ansari-Pour, N., Azimzadeh, S. & Mirzaie, M. A logic-based dynamic modeling approach to explicate the evolution of the central dogma of molecular biology. *PLoS One* **12**, e0189922 (2017).

22. Park, J. *et al.* Pan-RAF inhibitor LY3009120 is highly synergistic with low-dose cytarabine, but not azacitidine, in acute myeloid leukemia with RAS mutations. *Oncol. Lett.* **22**, 745 (2021).
23. Gong, S. *et al.* A human pan-cancer system analysis of procollagen-lysine, 2-oxoglutarate 5-dioxygenase 3 (PLOD3). *Int. J. Mol. Sci.* **22**, 9903 (2021).
24. Pinnelli, M. (2023).
25. Singh, R. *et al.* Reduction of Derlin activity suppresses Notch-dependent tumours in the C. elegans germ line. *PLoS Genet.* **17**, e1009687 (2021).
26. Guo, N. *et al.* Effects of neddylation and mTOR inhibition in acute myelogenous leukemia. *Transl. Oncol.* **12**, 602–613 (2019).
27. Chen, J. *et al.* Glioblastoma stem cell-specific histamine secretion drives pro-angiogenic tumor microenvironment remodeling. *Cell Stem Cell* **29**, 1531–1546.e7 (2022).
28. Lontos, K. *et al.* The role of Semaphorin 4D in bone remodeling and cancer metastasis. *Front. Endocrinol. (Lausanne)* **9**, 322 (2018).
29. Ye, Z.-W. *et al.* Protein disulfide isomerase family mediated redox regulation in cancer. *Adv. Cancer Res.* **160**, 83–106 (2023).
30. Bauer, T. M. & Murphy, E. Role of mitochondrial calcium and the permeability transition pore in regulating cell death. *Circ. Res.* **126**, 280–293 (2020).
31. Chigaev, A. Does aberrant membrane transport contribute to poor outcome in adult acute myeloid leukemia? *Front. Pharmacol.* **6**, 134 (2015).
32. Bialkowski, K. & Kasprzak, K. S. Inhibition of 8-oxo-2′-deoxyguanosine 5′-triphosphate pyrophosphohydrolase (8-oxo-dGTPase) activity of the antimutagenic human MTH1 protein by nucleoside 5 …. *Free Radic. Biol. Med.* (2003).
33. Tzeng, H.-P. *et al.* Dysferlin mediates the cytoprotective effects of TRAF2 following myocardial ischemia reperfusion injury. *J. Am. Heart Assoc.* **3**, e000662 (2014).
34. Bansal, D. & Campbell, K. P. Dysferlin and the plasma membrane repair in muscular dystrophy.

Trends Cell Biol. **14**, 206–213 (2004).

35. Sigaud, R. *et al.* The first-in-class ERK inhibitor ulixertinib shows promising activity in mitogen-activated protein kinase (MAPK)-driven pediatric low-grade glioma models. *Neuro. Oncol.* **25**, 566–579 (2023).
36. Bernecky, C., Herzog, F., Baumeister, W., Plitzko, J. M. & Cramer, P. Structure of transcribing mammalian RNA polymerase II. *Nature* **529**, 551–554 (2016).
37. Blom, A. M., Villoutreix, B. O. & Dahlbäck, B. Complement inhibitor C4b-binding protein-friend or foe in the innate immune system? *Mol. Immunol.* **40**, 1333–1346 (2004).
38. Kim, L. C., Song, L. & Haura, E. Src kinases as therapeutic targets for cancer. *Nat. Rev. Clin. Oncol.* **6**, 587–595 (2009).
39. Sánchez-Mendoza, S. E. & Rego, E. M. Targeting the mitochondria in acute myeloid leukemia. *Appl. Canc. Res.* **37**, (2017).
40. Borkar, R. M. *et al.* An evaluation of the CYP2D6 and CYP3A4 inhibition potential of metoprolol metabolites and their contribution to drug-drug and drug-herb interaction by LC-ESI/MS/MS. *Biomed Chromatogr* **30**, 1556–1572 (2016).
41. Tambe, M. *et al.* Pan-RAF inhibition induces apoptosis in acute myeloid leukemia cells and synergizes with BCL2 inhibition. *Leukemia* 1–11 (2020).
42. Khaliq, M. & Fallahi-Sichani, M. Epigenetic mechanisms of escape from BRAF oncogene dependency. *Cancers (Basel)* **11**, (2019).
43. Sauter, C. *et al.* Protein arginine methyltransferases as therapeutic targets in hematological malignancies. *Cancers (Basel)* **14**, (2022).
44. Chen, J.-N. *et al.* Arylurea derivatives: A class of potential cancer targeting agents. *Curr. Top. Med. Chem.* **17**, 3099–3130 (2017).
45. Daenthanasanmak, A. *et al.* Enhanced efficacy of JAK1 inhibitor with mTORC1/C2 targeting in smoldering/chronic adult T cell leukemia. *Transl. Oncol.* **14**, 100913 (2021).

46. He, X. *et al.* The comparative oncology of canine malignant melanoma in targeted therapy: A systematic review of in vitro experiments and animal model reports. *Int. J. Mol. Sci.* **25**, (2024).

47. Sztiller-Sikorska, M. & Czyż, M. Parthenolide as cooperating agent for anti-cancer treatment of various malignancies. *Pharmaceuticals (Basel)* **13**, (2020).

48. Potapova, T. *et al.* Distinct states of nucleolar stress induced by anticancer drugs. *eLife* **12**, (2023).

49. Lukey, M. J., Katt, W. P. & Cerione, R. A. Targeting amino acid metabolism for cancer therapy. *Drug Discov. Today* **22**, 796–804 (2017).

50. Grayson, A. K. Elucidating the role of JAK/STAT signalling in polycythaemia vera and essential thrombocythaemia using proteomics. (2018).

51. Greenfield, G., McPherson, S., Mills, K. & McMullin, M. F. The ruxolitinib effect: understanding how molecular pathogenesis and epigenetic dysregulation impact therapeutic efficacy in myeloproliferative neoplasms. *J. Transl. Med.* **16**, 360 (2018).

52. McKinnell, Z., Karel, D., Tuerff, D., Sh Abrahim, M. & Nassereddine, S. Acute myeloid leukemia following myeloproliferative neoplasms: A review of what we know, what we do not know, and emerging treatment strategies. *J. Hematol. (Brossard)* **11**, 197–209 (2022).

53. Habbel, J. *et al.* Inflammation-driven activation of JAK/STAT signaling reversibly accelerates acute myeloid leukemia in vitro. *Blood Adv.* **4**, 3000–3010 (2020).

54. Biswas, J., Boussi, L., Stein, E. & Abdel-Wahab, O. Aberrant pre-mRNA processing in cancer. *J. Exp. Med.* **221**, (2024).

55. Li, J. *et al.* Functional phosphoproteomics in cancer chemoresistance using CRISPR-mediated base editors. *Adv. Sci. (Weinh.)* **9**, e2200717 (2022).

56. Wang, Y., Yu, L., Ding, J. & Chen, Y. Iron metabolism in cancer. *Int. J. Mol. Sci.* **20**, 95 (2018).

57. Goodall, G. J. & Wickramasinghe, V. O. RNA in cancer. *Nat. Rev. Cancer* **21**, 22–36 (2021).

58. Yang, L. *et al.* Phase separation-competent FBL promotes early pre-rRNA processing and

translation in acute myeloid leukaemia. *Nat. Cell Biol.* **26**, 946–961 (2024).

59. Smirnova, T., Spertini, C. & Spertini, O. CSF1R Inhibition Combined with GM-CSF Reprograms Macrophages and Disrupts Protumoral Interplays with AML Cells. *Cancers (Basel)* **13**, (2021).
60. Fassl, A., Geng, Y. & Sicinski, P. CDK4 and CDK6 kinases: From basic science to cancer therapy. *Science* **375**, eabc1495 (2022).
61. Panina, S. B., Pei, J. & Kirienko, N. V. Mitochondrial metabolism as a target for acute myeloid leukemia treatment. *Cancer Metab.* **9**, 17 (2021).
62. Gold, S. & Shilatifard, A. Epigenetic therapies targeting histone lysine methylation: complex mechanisms and clinical challenges. *J. Clin. Invest.* **134**, (2024).
63. Kurzava, L. A. Epigenetic Regulation of Oncogenic Signaling Pathways in Breast Cancer in Response to Dietary Polyphenols. (2017).
64. Venkadakrishnan, V. B. PKN1 is a novel therapeutic target to block serum response factor-dependent androgen receptor action in advanced prostate cancer. (2020).
65. Singh, V. *et al.* Phosphorylation: Implications in cancer. *Protein J.* **36**, 1–6 (2017).
66. Nantavisai, S. *et al.* Systems biology analysis of osteogenic differentiation behavior by canine mesenchymal stem cells derived from bone marrow and dental pulp. *Sci. Rep.* **10**, (2020).
67. Hood, J. & Cheresh, D. Role of integrins in cell invasion and migration. *Nat. Rev. Cancer* **2**, 91–100 (2002).
68. Yue, J. & López, J. M. Understanding MAPK signaling pathways in apoptosis. *Int. J. Mol. Sci.* **21**, (2020).
69. Yan, M. & Jurasz, P. The role of platelets in the tumor microenvironment: From solid tumors to leukemia. *Biochim. Biophys. Acta* **1863**, 392–400 (2016).
70. Guarnera, L. *et al.* Microenvironment in acute myeloid leukemia: focus on senescence mechanisms, therapeutic interactions, and future directions. *Exp. Hematol.* **129**, 104118 (2024).

71. Zhang, M. *et al.* TGF-β signaling and resistance to cancer therapy. *Front. Cell Dev. Biol.* **9**, 786728 (2021).

72. Das, S., Somisetty, V. S., Ulven, S. M. & Matthews, J. Resveratrol and 3,3'-diindolylmethane differentially regulate aryl hydrocarbon receptor and estrogen receptor alpha activity through multiple transcriptomic targets in MCF-7 human breast cancer cells. *Int. J. Mol. Sci.* **24**, (2023).

73. Chan, M. K.-K. *et al.* TGF-β signaling networks in the tumor microenvironment. *Cancer Lett.* **550**, 215925 (2022).

74. Gelfo, V. *et al.* Roles of IL-1 in cancer: From tumor progression to resistance to targeted therapies. *Int. J. Mol. Sci.* **21**, 6009 (2020).

75. Fabbri, L., Chakraborty, A., Robert, C. & Vagner, S. The plasticity of mRNA translation during cancer progression and therapy resistance. *Nat. Rev. Cancer* **21**, 558–577 (2021).

76. Ganesan, R. *et al.* D-series Resolvins activate Phospholipase D in phagocytes during inflammation and resolution. *FASEB J.* **34**, 15888–15906 (2020).

77. Liu, G.-H., Chen, T., Zhang, X., Ma, X.-L. & Shi, H.-S. Small molecule inhibitors targeting the cancers. *MedComm* **3**, e181 (2022).

78. Knight, J. R. P. *et al.* Control of translation elongation in health and disease. *Dis. Model. Mech.* **13**, dmm043208 (2020).

79. Balzano, E., Pelliccia, F. & Giunta, S. Genome (in)stability at tandem repeats. *Semin. Cell Dev. Biol.* **113**, 97–112 (2021).

80. Pomeroy, A. E., Schmidt, E. V., Sorger, P. K. & Palmer, A. C. Drug independence and the curability of cancer by combination chemotherapy. *Trends Cancer Res.* **8**, 915–929 (2022).

81. He, L. *et al.* Methods for High-throughput Drug Combination Screening and Synergy Scoring. *Methods Mol. Biol.* **1711**, 351–398 (2018).

82. Arnone, M. *et al.* Acute myeloid leukemia stem cells: The challenges of phenotypic heterogeneity. *Cancers (Basel)* **12**, (2020).

83. Filì, C. *et al.* Efficacy and toxicity of Decitabine in patients with acute myeloid leukemia (AML): A multicenter real-world experience. *Leuk. Res.* **76**, 33–38 (2019).

84. Saei, A. A. *et al.* Mapping the GALNT1 substrate landscape with versatile proteomics tools. (2022) doi:10.1101/2022.08.24.505189.

85. Saei, A. A. *et al.* System-wide identification and prioritization of enzyme substrates by thermal analysis. *Nat Commun* **12**, 1296 (2021).

86. Sabatier, P. *et al.* An integrative proteomics method identifies a regulator of translation during stem cell maintenance and differentiation. *Nat Commun* **12**, 6558 (2021).